Work statistics for quantum spin chains: Characterizing quantum phase transitions, benchmarking time evolution, and examining passivity of quantum states

Feng-Li Lin [1,*] and Ching-Yu Huang [2,†]

[1]*Department of Physics, National Taiwan Normal University, Taipei, 11677, Taiwan*
[2]*Department of Applied Physics, Tunghai University, Taichung, 40704, Taiwan*

(Received 21 December 2023; accepted 26 April 2024; published 14 May 2024)

We study three aspects of work statistics in the context of the fluctuation theorem for quantum spin chains up to 1024 sites by numerical methods based on matrix-product states (MPSs). First, we use our numerical method to evaluate the moments/cumulants of work done by the sudden quench process on the Ising or Haldane spin chains, and we study their behaviors across the quantum phase transitions. Our results show that, up to the fourth cumulant, the work statistics can indicate the quantum phase transition characterized by the local order parameters but barely for purely topological phase transitions. Second, we propose to use the fluctuation theorem, such as Jarzynski's equality, which relates the real-time correlator to the ratio of the thermal partition functions, as a benchmark indicator for the numerical real-time evolving methods. Third, we study the passivity of ground and thermal states of quantum spin chains under some cyclic impulse processes. We show that the passivity of thermal states and ground states under the Hermitian actions is ensured by the second laws and variational principles, respectively, and we also verify this by numerical calculations. In addition, we also consider the passivity of ground states under non-Hermitian actions, for which the variational principle cannot be applied. Despite that, we find no violation of passivity from our numerical results for all the cases considered in the Ising and Haldane chains. Overall, we demonstrate that the work statistics for the sudden quench and impulse processes can be evaluated precisely by the numerical MPS method to characterize quantum phase transitions and examine the passivity of quantum states. We also propose to exploit the universality of the fluctuation theorem to benchmark the numerical real-time evolutions in an algorithmic and model-independent way.

DOI: 10.1103/PhysRevResearch.6.023169

I. INTRODUCTION

Motivated by the progress of quantum simulations in cold-atom experiments [1–5] and the theoretical understanding of the thermalization of isolated quantum systems [6–8], the nonequilibrium dynamics of quantum systems have been studied extensively [9–13]. A system can be driven into nonequilibrium simply by introducing a time-dependent interaction or a time-dependent coupling constant, and the system can return to equilibrium after turning off the time dependence of the coupling. For a many-body system, obtaining the exact dynamical evolution is generally difficult. Given a numerical method of evaluating the dynamical evolution, finding a way to estimate the numerical accuracy becomes a challenging task, especially for a system without prior knowledge of the exact dynamics. One would expect that the numerical error accumulates as the system evolves. Therefore, a reliable real-time error estimator will help compare the numerical results with the experimental ones, such as the quantum simulation.

For nonequilibrium dynamics of an isolated quantum system, one would expect that the underlying microreversibility should manifest in some way, in contrast with the macroscopic second law of thermodynamics. Indeed, equality relations exist, collectively known as fluctuation theorem [14–23], for such a manifestation. The work done in a nonequilibrium process is not a state variable and will depend on the path connecting the initial and final state. The fluctuation theorem relates the average work to the free-energy difference between the initial and final states. To calculate the average work or the higher moments, one can construct the corresponding characteristic function (or generating function of work statistics), which can be rewritten as the real-time correlation function [17,19,24]. This characteristic function of work takes a form similar to the out-of-time-ordered correlator (OTOC) in characterizing the quantum chaos [25–27]. In general, one needs to adopt some numerical method to calculate this generating function or some OTOC-like quantities involving nonequilibrium dynamical evaluation, which may be spoiled by the accumulation of numerical errors. On the other hand, the difference in free energy only depends on the initial and final states. It will require disproportionately less numerical effort than that needed for the characteristic function. Exploiting a feature of such disproportionality in the numerical efforts on both sides of the fluctuation theorem, one can use it to

*fengli.lin@gmail.com
†cyhuangphy@thu.edu.tw

monitor the accuracy of any numerical method for evaluating the real-time nonequilibrium dynamical evolution of a quantum system. In recent works [28], a numerical method based on the matrix-product-state (MPS) approach [29,30] was adopted to evaluate the characteristic function for Ising spin chains and to verify the fluctuation theorem; see also [31] for a similar method for evaluating the heat statistics of open systems. This method can also be generalized to two-dimensional spin lattices, called the tensor-network state (TNS) [32]. In this paper, we will adopt the MPS method to evaluate the characteristic function of other quantum spin chains, and we will use the fluctuation theorem to benchmark the capability of these numerical time-evolving methods.

Another interesting aspect of work statistics is characterizing the (dynamical) quantum phase transitions (QPTs). This was first demonstrated in [33] for the Ising chain and later in [34] for the random matrix models under a sudden quench process, i.e., with a sudden change of the Hamiltonian, for which the work characteristic function is related to the Loschmidt echo. Moreover, the average work done on the isolated system measures the expectation value of the jump of the Hamiltonian across the quenching point with respect to the initial state. Then, a similar trick is applied to show the universal scaling behavior of the kink statistics for the dynamical quantum phase transition under the Kibble-Zurek mechanism (KZM) for the (Ising) spin chains [35–38], and for the Kitaev honeycomb model [39]. This approach to characterizing QPTs by work statistics is extended to the (exactly solvable) spin/fermion chain models under the nonquench processes [35,40,41].

It is also known that entanglement structures like entanglement entropy can also characterize QPTs by showing a discontinuity at critical points in many cases of QPTs; e.g., see [42,43]. As both the entanglement entropy and the work statistics can be encoded as some combinations of multipoint correlations, this may explain why both can characterize QPTs through some singular multipoint correlations. This perspective has been explored in [44] for the fermionic Hubbard model with random impurities. It was shown that the entanglement is minimized while the work average is maximized at the critical point, but the second moment of work vanishes. In this paper, we will study this issue further for Ising and Haldane chains.

When considering the quantum phase transition, the initial state is the ground state. After the sudden quench, it becomes a linear combination of the various excited states of the new Hamiltonian close in energy. If both initial and final Hamiltonians are noncritical and gapped, then only the gapped excited states with their energies less than the average work done on the system can be induced. However, if the final Hamiltonian happens to be at the quantum critical point, it describes a gapless system, and an infinite number of gapless excitations will be induced. We expect the work statistics to differ from those for the noncritical cases because this large number of gapless excitations will provide more dynamic paths for the quenching process for retrieving a definite amount of work. This implies that the average work excitation can display discontinuous behavior when the sudden quench connects a noncritical Hamiltonian to a critical one. In this sense, the work statistics, i.e., the average work done or the higher cumulants, can be adopted to characterize the quantum phase transitions, i.e., as an order parameter. Since the above reasoning concerns only the gapless feature of the critical systems, it can work for both the quantum phase transition of the Landau-Ginzburg type due to spontaneously-symmetry breaking (SSB), or the topological type characterized by nonlocal order parameters. Finding the appropriate order parameter to indicate the topological phase transition is usually more difficult. In this paper, we will explore the power of the numerical MPS-based algorithm to evaluate the moments/cumulants of work statistics and demonstrate their capability and limitations in characterizing the QPTs of the quantum Ising and Haldane chains. With the help of the quantum-state RG of MPSs, we can evaluate the work statistics for chains up to 1024 sites. This will effectively suppress the finite-size effect, especially when near the quantum critical point.

Finally, we would like to study the issue of the passivity of ground states of quantum spin chains under cyclic impulse processes. It had been known that the relativistic thermal states are always passive, i.e., no work can be extracted from the system in any cyclic process [45–47]. We first show that the passivity of thermal states is guaranteed by the fluctuation theorem or, equivalently, the second law of thermodynamics. It is also straightforward to see that the passivity of ground states under Hermitian action is guaranteed by the variational principle, i.e., the ground state has the lowest energy. However, the variational principle fails to ensure the passivity of the ground states if the action for driving nonequilibrium is non-Hermitian. We then adopt the MPS numerical method to examine the passivity for such cases. In all cases we checked, we found no active ground states even under non-Hermitian action. In addition, the patterns of average work extraction show some interesting features.

Based on the work statistics and the fluctuation theorem, we will use reliable numerical methods to investigate the above three aspects of the quantum spin lattice models in this paper: characterizing the quantum phase transitions, benchmarking the accuracy of the numerical real-time evolution, and examining the passivity. These studies enlarge the perspective of the work done and the fluctuation theorem. In summary, in this work we will demonstrate the power of the numerical MPS method in evaluating the work statistics precisely enough to characterize the quantum phase transitions and examine the passivity of quantum states, even for the non-Hermitian actions. Moreover, we will also show how to exploit the simplicity and universality of the fluctuation theorem to benchmark the numerical real-time evolutions for generic models and numerical algorithms.

The rest of the paper is organized as follows. For completeness, in the next section we briefly review the basics of work statistics and the fluctuation theorem and elaborate on the theoretical frameworks of the three aspects of work statistics that we address in this paper. In Sec. III, we review the numerical methods for evaluating the real-time correlators based on MPSs and then apply them to evaluate the generating function of work statistics and the expectation values of physical observables. In Sec. IV, we apply the above numerical methods to Ising-like and Haldane-like spin chains. Our numerical results demonstrate that the work statistics from the

sudden quench can be used to characterize the quantum phase transitions for all spin models. In Sec. V, we show the results of using Jarzynski's equality as the benchmark to gauge the numerical accuracy of the real-time evolving methods. In Sec. VI, we present our results of examining the passivity of the ground states of the quantum spin chains under both Hermitian and non-Hermitian actions. Finally, in Sec. VII, we summarize our work and discuss the possible extensions. Some numerical consistency checks and supplements are presented in the Appendixes.

II. WORK STATISTICS AND ITS APPLICATIONS

A. Work statistics and fluctuation theorem

We first give a brief sketch of the basics of work statistics in the context of the fluctuation theorem, which provides an elegant framework for describing and characterizing thermal or quantum fluctuations in statistical mechanics.

Unlike some conservative quantities, work is not a state variable, and it will depend on the microscopic details/paths of the nonequilibrium process. In short, work is a random variable and is characterized by a distribution function defined for work statistics as follows:

$$p(W) = \sum_{a,b} \delta(W - [E_b(t_f) - E_a(0)])\, p(b, t_f|a)\; p_a, \quad (1)$$

where $p(b, t_f|a)$ is the transition probability from the energy eigenstate $|a\rangle$ of energy $E_a(0)$ at time $t = 0$ to another eigenstate $|b, t_f\rangle$ of energy $E_b(t_f)$. This nonequilibrium process is driven by a time-dependent Hamiltonian $H(t)$ from an initial state of density matrix $\rho(0) = \sum_a p_a|a\rangle\langle a|$, with $H(0)\,|a\rangle = E_a(0)\,|a\rangle$ and $H(t_f)\,|b, t_f\rangle = E_b(t_f)\,|b, t_f\rangle$. Thus, we have

$$p(b, t_f|a) = |\langle b, t_f|U(t_f)|a\rangle|^2 = |\langle a|U^\dagger(t_f)|b, t_f\rangle|^2 \quad (2)$$

with $U(t_f) = \mathcal{T} e^{-i\int_0^{t_f} H(t)dt}$. For simplicity, in this paper we will only consider the cases with $H(t) = H_0 + \lambda(t)V$ with time-independent H_0 and V, so that $[H(t), H(t')] = 0$ and the time-ordering symbol $\mathcal{T}$ in $U(t_f)$ can be omitted. Moreover, in general we will allow for non-Hermitian $H(t)$ so that $U(t_f)$ can be nonunitary, i.e., $U^\dagger(t_f) \neq U^{-1}(t_f)$. The last equality implies detailed balance or microreversibility. Similarly, one can define the work statistics from the "reverse process" with an "initial state" of the density matrix $\rho(0) = \sum_m q_m|m, t_f\rangle\langle m, t_f|$ as follows:

$$\tilde{p}(-W) = \sum_{a,b} \delta(-W + [E_b(0) - E_a(0)])\, \tilde{p}(a|b, t_f)\, q_b, \quad (3)$$

where the transition probability for the reverse process is $\tilde{p}(a|b, t_f) = |\langle a|U^\dagger(t_f)|b, t_f\rangle|^2 = p(b, t_f|a)$, with the last equality ensured by microreversibility.

The fluctuation theorem is usually formulated for the canonical initial and final states, i.e., $p_a = e^{-\beta[E_a(0)-F(0)]}$ and $q_b = e^{-\beta[E_b(t_f)-F(t_f)]}$, with $\beta = \frac{1}{k_B T}$ the inverse temperature, and $F(0)$ and $F(t_f)$ are the free energy for the initial and final states, which are defined by the partition functions $Z(0) = e^{-\beta F(0)}$ and $Z(t_f) = e^{-\beta F(t_f)}$, respectively. Then, the fluctuation theorem taking the form of Crooks' relation [16] can be obtained by construction from Eqs. (1)–(3), and it reads

$$p(W)\, e^{-\beta(W-\Delta F)} = \tilde{p}(-W), \quad (4)$$

where $\Delta F = F(t_f) - F(0)$. Integrating this relation over W, we can obtain Jarzynski's equality [14,17],

$$\overline{e^{-\beta W}} = e^{-\beta \Delta F}, \quad (5)$$

where the "overline" denotes the average over work W. Using Jensen's inequality, Jarzynski's equality can yield the second law: $\Delta S := \overline{W} - \Delta F \geqslant 0$. The fluctuation theorem for more general quantum processes and end states can be found in [20,22,23].

From the work statistics, we can define the corresponding characteristic function as

$$G(u) = \int dW\, e^{iuW} p(W). \quad (6)$$

This function is the generating function of the moments of work done, e.g.,

$$\overline{W} = \frac{1}{i} \lim_{u\to 0} \frac{\partial \ln G(u)}{\partial u}, \quad (7)$$

$$\sigma_W^2 := \overline{W^2} - \overline{W}^2 = -\lim_{u\to 0} \frac{\partial^2 \ln G(u)}{\partial u^2}. \quad (8)$$

For simplicity, later we will mostly adopt $\overline{W} = \lim_{s\to 0} \frac{\partial G(-is)}{\partial s}$ since $G(-is)$ is real and $G(0) = 1$.

Moreover, Jarzynski's equality can be expressed as follows:

$$G(i\beta) = e^{-\beta \Delta F}. \quad (9)$$

After some straightforward manipulation, the work characteristic function $G(u)$ of a nonequilibrium process, which drives the initial state $\rho(0)$ by a time-dependent Hamiltonian $H(t)$ during the time interval $[0, t_f]$, can be put into the following form [19]:

$$G(u; t_f) = \frac{\mathrm{Tr}[\, U^\dagger(t_f) e^{iuH(t_f)} U(t_f) e^{-iuH(0)} \rho(0)\,]}{\mathrm{Tr}[\, U^\dagger(t_f) U(t_f) \rho(0)\,]}. \quad (10)$$

The denominator is unity for unitary $U(t_f)$ [or hermitian $H(t)$]. The expression of Eq. (10) can be recast into the real-time correlation function on the extended Schwinger-Keldysh contour [24] so that techniques of open system dynamics can be adopted. We usually omit t_f and write $G(u)$.

To be specific, in this paper we will only consider the time-dependent Hamiltonian of the following form:

$$H(t) = H_0 + \lambda(t)V, \quad (11)$$

where we choose the initial Hamiltonian $H_0 = H(0^-)$ to be time-independent and Hermitian; however, the driving operator V is time-independent but could be non-Hermitian. If V is non-Hermitian, then $U(t)$ is nonunitary so that the denominator of Eq. (10) is not unity. An initial state ρ_0, which is taken to be either the thermal state or the ground state of H_0, will be driven away from equilibrium due to the nontrivial time dependence of the coupling constant $\lambda(t)$. The notations 0^- and 0^+ used later denote the moments right before and after $t = 0$, respectively.

We will consider two particular nonequilibrium processes in the following:

(i) Sudden quench process with

$$\lambda(t) = \Delta\lambda\Theta(t), \quad (12)$$

where $\Theta(t)$ is the Heaviside step function, and $\Delta\lambda$ is a constant. For such a process, $U(t_f)|_{t_f\to 0} = 1$, $H(0^-) = H_0$, and $H(0^+) = H_0 + \Delta\lambda V$.

(ii) Impulse process with

$$\lambda(t) = \lambda\delta(t), \tag{13}$$

where $\delta(t)$ is the Dirac delta function and λ is a constant. Compared to a sudden quench process, the coupling constant is turned off right before and after the impulse so that $H(0^-) = H(0^+) = H_0$. Thus, this process can be considered cyclic and will be implemented to study passivity.

In both kinds of processes, we will find that the average work done $\overline{W}$ extracted from $G(u)$ can characterize (quantum) phase transitions.

B. Benchmark the numerical real-time evolution

Jarzynski's equality shown in Eq. (9) is an interesting relationship that relates a real-time correlator to the ratio of the partition functions, i.e., $e^{-\beta\Delta F} = \frac{Z(t_f)}{Z(0)}$. There is usually no analytical method to calculate the real-time correlators such as $G(u)$ of Eq. (10) of a many-body system even though there might be some analytical ways of calculating the partition function. Even relying on the numerical method to evaluate the real-time correlators, the numerical errors accumulate more as the evolution continues. On the other hand, the partition function is a stationary quantity free of the accumulated error. Therefore, we can characterize the accumulated error by defining the following ratio:

$$R(t_f) = \frac{G(i\beta)}{e^{-\beta\Delta F}} = G(i\beta)\frac{Z(0)}{Z(t_f)}, \tag{14}$$

which is the ratio of the left-hand side to the right-hand side of Jarzynski's equality and is a function of evolution time t_f.

By monitoring the deviation of $R(t_f)$ from unity, one can estimate the numerical error accumulation of a numerical method for real-time evolution in a first-principles way without the need to compare with the analytical or other numerical methods. For different numerical methods for real-time evolution, we can compare the deviations of their $R(t_f)$ from unity for different numerical methods for real-time evolution to benchmark their performances. Later, we will demonstrate benchmarking for the numerical methods adopted in this paper.

C. Work done by sudden quench and phase transition

In general, the work statistics or its characteristic function for the many-body system is difficult to evaluate for the complication of real-time dynamics. However, to characterize the phase transition, we can bypass the difficulty by just considering the work done by a sudden quench implemented by the Hamiltonian of Eqs. (11) and (12). Denote the ground state of H_0 by $\rho_0 \equiv |0\rangle\langle 0|$, and the Hamiltonian after quench by H_+, i.e., $H_+ \equiv H_0 + \Delta\lambda V$. Then the characteristic function can be simplified as follows:

$$\lim_{t_f\to 0^+} G(u) = \mathrm{Tr}[e^{-iuH_0}\rho_0 e^{iuH_+}], \tag{15}$$

which yields moments and the first few cumulants of the work done as follows:

$$\overline{W^m} = (\Delta\lambda)^m\ \langle 0|V^m|0\rangle, \tag{16}$$

$$\begin{aligned}\sigma_W^2 &= \langle 0|H_+^2|0\rangle - \langle 0|H_+|0\rangle^2,\\ &= (\Delta\lambda)^2(\langle 0|V^2|0\rangle - \langle 0|V|0\rangle^2),\end{aligned} \tag{17}$$

$$\kappa_3 = \overline{W^3} - 3\overline{W^2}\,\overline{W} + \overline{W}^3, \tag{18}$$

$$\kappa_4 = \overline{W^4} - 4\overline{W^3}\,\overline{W} - 3\overline{W^2}^2 + 12\overline{W^2}\,\overline{W}^2 - 6\overline{W}^4. \tag{19}$$

The quantity $\overline{W}$, as shown for the sudden quench, measures the energy of the "excited state" $|0\rangle$ with respect to H_+, while the quantity σ_W measures the corresponding fluctuation of $\Delta H = \Delta\lambda V$. Thus, $\overline{W}$ (or σ_W^2) could act as a local order parameter to characterize the quantum phase transition while tuning H_0. From Eq. (16) we can also calculate the higher moments $\overline{W^m}$ or higher cumulants κ_m for the sudden quench in terms of the expectation value of higher order V^m's.

We now elaborate on why the quantities in Eqs. (16) and (17) can be used as the order parameter to characterize the phase transition. First, suppose the initial and final states are Gibbs states related by unitary evolution. In that case, the Hamiltonian can also be understood as the modular Hamiltonian, i.e., $H_{\mathrm{mod}} = -\log\rho$. In this case, $\overline{W}$ can be rewritten as the relative entropy S_{rel} [20], i.e.,

$$\overline{W} = \mathrm{Tr}[\,\rho_-^{\mathrm{G}}\Delta H_{\mathrm{mod}}\,] = S_{\mathrm{rel}}(\rho_-^{\mathrm{G}}|\rho_+^{\mathrm{G}}), \tag{20}$$

where $\rho_{-,+}^{\mathrm{G}}$ are the Gibbs states before and after quench, respectively. In this case, $\overline{W}$ measures the distance between the initial and final Gibbs states. For the case we consider, the initial and final states are pure, and $\overline{W}$ is no longer equivalent to the relative entropy. However, as explained below, $\overline{W}$ can still be used to distinguish pure states, especially the critical and noncritical ones.

The phase transition is usually characterized by the order parameter, which is the expectation value of some local or nonlocal observables. We can decompose the Hamiltonian $H_+ = \sum_f E_{f^+}|f^+\rangle\langle f^+|$, so that Eq. (16) with $m = 1$ can be rewritten as

$$\overline{W} = \sum_f E_{f^+}|\langle 0|f^+\rangle|^2 = \overline{E_{f^+}}. \tag{21}$$

The average work done $\overline{W}$ can be seen as the expectation value of E_{f^+} with its probability measure given by $p(f) = |\langle 0|f^+\rangle|^2$. We will tune some coupling in H_0 over a range covering different phases. Again, $|0\rangle$ looks like the excited state to H_+. When H_0 and H_+ are in the same phase, we expect $|0^+\rangle \approx |0\rangle$ so that $p(f) = \delta_{f,0}$ and $\overline{W} \simeq E_{0^+}|\langle 0|0^+\rangle|^2 \simeq E_{0^+}$. On the other hand, if they are in different phases, we should not expect a sharp distribution for $p(f)$, and $\overline{W}$ will be quite different from E_{0^+} due to the incoherent average. For example, when H_+ is the gapless critical Hamiltonian at the quantum critical point, we expect the emergence of a dense set of degenerate gapless states denoted as $\{0_c^+\}$ such that the density of ground states $p(0^+) = \sum_{\{0_c^+\}} p(c) < 1$, which is quite different from the case of noncritical gapped H_+ with $p(0^+) \simeq 1$. This then induces a sudden jump of $\overline{W}$ from $\overline{W} \simeq E_0^+$ to the

incoherent average $\overline{W} \simeq E_{0^+} \sum_{\{0_c^+\}} p(0_c^+) + \sum_{f\neq\{0^+\}} p(f)E_f$. Therefore, $\overline{W}$ can be used as an order parameter for the phase transition. Similar arguments apply for σ_W^2 or higher moments/cumulants. Some preliminary study of $p(f)$ for a quantum Ising chain under sudden quench by the exact diagonalization (ED) method is done in Appendix A, and the result is shown in Fig. 11 therein.

D. Passivity of a quantum state: Thermal or ground states

A quantum state is called passive if there is no work extraction, i.e., $\overline{W} \geqslant 0$, under a cyclic process defined by $H(t_f) = H(0)$. It was shown that the KMS state [48,49], i.e., the thermal vacuum state for a relativistic quantum field theory, is passive [45–47]. Even though there is no general criterion for checking the passivity of a generic quantum state, it can be argued from the fluctuation theorem as follows. For a cyclic process, we shall expect $\Delta F = 0$ so that the fluctuation theorem becomes $\overline{e^{-\beta W}}|_{\text{cyclic}} = 1$. By Jensen's inequality, this implies a second-law statement

$$\Delta S = \overline{W}|_{\text{cyclic}} \geqslant 0. \tag{22}$$

Therefore, the fluctuation theorem guarantees the thermal states' passivity, thus the second law. Since the second law is established only in the thermodynamic limit, there is evidence that the thermal-like states of finite systems under some peculiar process can be active [50–52].

Based on the above result, it is worth mentioning the study in [53], which considered the passivity of the energy eigenstates of Ising chains under the action of local Hermitian operations. By adopting the eigenstate thermalization hypothesis [8,54,55], an energy eigenstate locally looks like a thermal state, e.g., the reduced density matrix of a local region is approximately a thermal one with some effective temperature. Thus, based on the passivity of the thermal state and ETH, an energy eigenstate will probably be passive under the action of local unitary operations. In [53], it was shown that all the energy eigenstates are passive under local operations for nonintegrable Ising chains of finite size, while most energy eigenstates are passive for integrable Ising chains. This is consistent with the fact that ETH holds only weakly for integrable systems; see, e.g., [56–58]. The above result could also help to explain the passivity of the ground states studied below and imply a negative effective temperature.

Intuitively, the ground states should be passive because the operation V excites the ground state to those with larger energies so that one cannot extract energy from the ground state. We can check passivity by first obtaining the average work extraction $W_{\text{ext}}^{\text{cyclic}} \equiv -\overline{W}$ for the cyclic process with $H(t_f) = H(0) := H_0$ from the characteristic function of Eq. (10), i.e.,

$$W_{\text{ext}}^{\text{cyclic}} = \text{Tr}[H_0\rho_1] - \text{Tr}[H_0\rho_2], \tag{23}$$

where

$$\rho_1 := \frac{\rho_0 U^\dagger(t_f)U(t_f)}{\text{Tr}[\,\rho_0 U^\dagger(t_f)U(t_f)\,]}, \tag{24}$$

$$\rho_2 := \frac{U(t_f)\rho_0 U^\dagger(t_f)}{\text{Tr}[\,\rho_0 U^\dagger(t_f)U(t_f)\,]}. \tag{25}$$

Note that $\text{Tr}\rho_1 = \text{Tr}\rho_2 = 1$. Moreover, if $U(t_f)$ is unitary, i.e., $U^\dagger(t_f) = U^{-1}(t_f)$, then $\rho_1 = \rho_0$ and $\rho_2 = U(t_f)\rho_0 U^\dagger(t_f)$, so that Eq. (23) can be reduced to

$$W_{\text{ext}}^{\text{cyclic}} = \text{Tr}[H_0\rho_0] - \text{Tr}[H_0 U(t_f)\rho_0 U^\dagger(t_f)], \tag{26}$$

which is simply the energy difference between the ground state ρ_0 and the excited state $U(t_f)\rho_0 U^\dagger(t_f)$. Thus, in such cases, the passivity of the ground state is guaranteed if the variational principle holds. On the other hand, if $U(t_f)$ is nonunitary, then $\rho_1 \neq \rho_0$ even though ρ_2 resembles an excited state under nonunitary evolution. Therefore, the negativity of $W_{\text{ext}}^{\text{cyclic}}$ of Eq. (23) can no longer be ensured by the variational principle.

We can conclude from the above discussions that the variational principle generally ensures the ground state's passivity. In this work, we will verify this by numerical calculation and explore its possible violations by considering the cases of non-Hermitian V so that the variational principle cannot be applied to guarantee the negativity of $W_{\text{ext}}^{\text{cyclic}}$ of Eq. (23).

For simplicity and numerical implementation, we will only consider the impulse cyclic processes, i.e., with $\lambda(t)$ given by Eq. (13), for which we have

$$\lim_{t_f\to 0^+} U(t_f) = \lim_{t_f\to 0^+} e^{-i\int_{0^-}^{t_f} dt[H_0+\lambda\delta(t)V]} = e^{-i\lambda V}. \tag{27}$$

This yields

$$G(u) = \frac{\text{Tr}[e^{i\lambda V^\dagger} e^{iuH_0} e^{-i\lambda V} e^{-iuH_0}\rho_0]}{\text{Tr}[e^{i\lambda V^\dagger} e^{-i\lambda V}\rho_0]}. \tag{28}$$

It turns out that we can easily implement the MPS formalism for spin-chain models to evaluate the right side of Eq. (28) numerically and then extract $W_{\text{ext}}^{\text{impulse}}$ from the results. Alternatively, the average work extraction can also be obtained from Eqs. (23)–(25) by replacing $U(t_f)$ with $e^{-i\lambda V}$ and $U^\dagger(t_f)$ with $e^{i\lambda V^\dagger}$.

It is easy to see that $W_{\text{ext}}^{\text{impulse}}$ vanishes exactly if $[V, H_0] = 0$. Otherwise, by assuming $H_0|0\rangle = 0$ and taking a small $|\lambda|$ expansion up to $O(\lambda^4)$, we have

$$\begin{aligned} W_{\text{ext}}^{\text{impulse}} =& -\lambda^2\,\langle V^\dagger H_0 V\rangle + \frac{i}{2}\lambda^3[\langle V^\dagger H_0 V^2 - V^{\dagger 2} H_0 V\rangle \\ &+ 2\langle V^\dagger - V\rangle\langle V^\dagger H_0 V\rangle] \\ &- \frac{1}{6}\lambda^4\Big[\Big\langle \frac{3}{2}V^{\dagger 2}H_0V^2 - V^{\dagger 3}H_0V - V^\dagger H_0 V^3\Big\rangle \\ &- 3\langle V^\dagger - V\rangle\langle V^\dagger H_0 V^2 - V^{\dagger 2}H_0V\rangle \\ &+ 3\langle V^\dagger H_0 V\rangle\langle V^{\dagger 2} + V^2 - 2V^\dagger V\rangle\Big], \end{aligned} \tag{29}$$

where we abbreviated $\langle 0|\cdots|0\rangle$ as $\langle\cdots\rangle$. We see that the $O(\lambda)$ term is absent, so that at $O(\lambda^2)$, $W_{\text{ext}}^{\text{impulse}}$ is independent of the sign of λ. Note also that the last terms in each order shown above all vanish for $V^\dagger = V$. Although this expression contains terms with an imaginary i factor, they are always associated with the expectation values of anti-Hermitian operators, so the overall expression is a real quantity.

In addition, due to the peculiarity of the impulse process, there are some interesting features of $W_{\text{ext}}^{\text{impulse}}$. First, if $V = \sum_k \sigma_i^a$ for the spin-1/2 chain, with σ_k^a for $a = 1, 2, 3$, are the

Pauli matrices for the spin operator at site k, then $e^{-i\lambda V} = \prod_k e^{-i\lambda\sigma_k^a} = \prod_k(\cos\lambda - i\sigma_k^a \sin\lambda)$, which is periodic in λ. The resultant $W_{\text{ext}}^{\text{impulse}}$ is then also periodic in λ. Secondly, if $V = i\sum_k \sigma_i^a$ for the spin-1/2 chain, similar to but not the same as the Hermitian case, $e^{-i\lambda V} = e^{i\lambda V^\dagger} = \prod_k e^{\lambda\sigma_k^a} = \prod_k(\cosh\lambda + \sigma_k^a \sinh\lambda)$. Using this to evaluate $W_{\text{ext}}^{\text{impulse}}$ and using the fact that $H_0|0\rangle = 0$, we can obtain

$$\lim_{\lambda\to\infty} W_{\text{ext}}^{\text{impulse}} = -\frac{\left\langle \prod_k (1+\sigma_k^a) H_0 \prod_j (1+\sigma_j^a)\right\rangle}{2\left\langle \prod_k (1+\sigma_k^a)\right\rangle}, \quad (30)$$

which saturates to a negative finite constant as $\lambda \to \infty$. Note that the negativity is ensured by the variational principle and $|\langle\sigma_k^a\rangle| \leqslant 1$. The peculiar features for both types of V of spin-1/2 chains are due to the highly nonadiabatic nature of the impulse process. Similar conclusions can be drawn for the spin-1 chain with some specific V composed of the sum of site-spin operators.

From the above discussion, we see that the passivity (or the negativity of $W_{\text{ext}}^{\text{impulse}}$) is guaranteed by the variational principle in the small-λ regime regardless of whether V is Hermitian or not. Therefore, when exploring the possibility of violating the passivity of the ground states for the non-Hermitian V, we will investigate the large-λ regime, to which the variational principle cannot be directly applied.

Finally, we comment on the possible physical realization of a non-Hermitian operation, although our consideration in this work is somewhat academic. There are ways to realize non-Hermitian actions. One way is to drop the quantum jump term in the Lindblad master equation for the open quantum system by choosing the proper Lindblad operator, and the resultant equation describes the Heisenberg evolution of the density matrix operator by a non-Hermitian Hamiltonian; see, e.g., [59]. This can be alternatively realized on quantum circuits by probability quantum computing with suitably dilated Hilbert space; see [60]. Or, one can introduce the non-Hermitian interaction in the context of $\mathcal{PT}$-symmetry. For the Ising chain, it is equivalent to introducing an imaginary magnetic field; see, e.g., [61].

III. NUMERICAL METHODS FOR IMAGINARY- AND REAL-TIME EVOLUTION

To calculate the work statistics, we must evaluate the associated generating function, i.e., the real-time correlator of the characteristic function, Eq. (10). Even for a quenching process, it still involves a nontrivial vacuum expectation value (VEV) as given by Eq. (15) or the average work done given by Eq. (16). This is usually a challenging task for many-body systems. To study the work statistics for various many-body quantum systems, a recent work [28] has adopted the numerical method based on a matrix-product state (MPS) [29,30] for quantum spin chains. This method is called time-evolving block decimation (TEBD) [62,63] to use for the real-time evolution or evaluation of the VEV by its imaginary-time evolution. Below, we will review the basic ideas of this method and mention its application for our purposes.

Moreover, Jarzynski's equality (9) relates a real-time correlator to the ratio of the partition functions of thermal states, which is far easier to evaluate than the former. Therefore, we can use Jarzynski's equality to gauge the accuracy of the numerical real-time evolution and serve as the benchmark for a given numerical method for real-time evolution. In the next section, we will benchmark the TEBD and the exact diagonalization (ED).

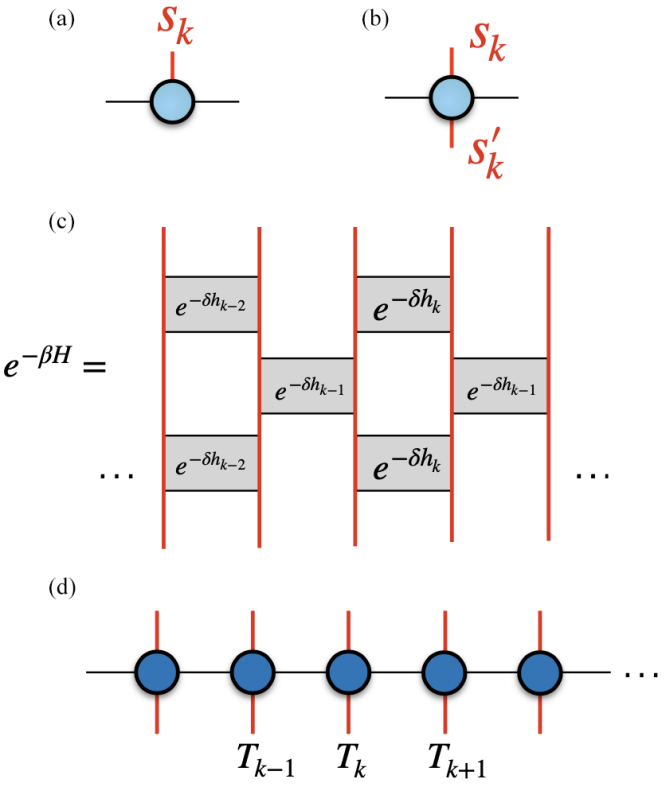

FIG. 1. (a) Symbol for matrix product state (MPS) structure. (b) Symbol for matrix product operator (MPO) structure. (c) MPO representation of the operator $e^{-\beta H}$ for a quantum system with nearest-neighbor interaction via the TEBD algorithm. (d) MPO representation of approximated $e^{-\beta H}$.

A. Matrix product states

For the one-dimensional quantum many-body systems, the ground states could be expressed in terms of a matrix product state (MPS), which can be expressed as

$$|\psi\rangle = \sum_{s_1,s_2,\ldots,s_n} \text{tTr}[A^{s_1}A^{s_2}\cdots A^{s_n}]|s_1 s_2 \cdots s_n\rangle, \quad (31)$$

where $s_k = 1, 2, \ldots, d_s$ for $k = 1, 2, \ldots, n$, with n the number of sites of the spin chain, and A^{s_i} is the on-site tensor. For example, $A_{l,r}^{s_k}$ is a rank-3 tensor for 1D MPS as shown in Fig. 1(a). Moreover, we can also generalize this idea to represent quantum many-body operators, called matrix product operators (MPOs), as shown in Fig. 1(b). We call d_s the physical dimension and χ_{cut} the bond dimension. tTr is to sum over all indices of tensors. Depending on the situation, we should tune χ_{cut} to capture the ground state's essential feature fully. Despite that, the χ_{cut} generally required for a good approximation of ground states still yields a more efficient representation of the quantum ground states than the typical dimensions of d_s^N. The validity of the MPS ansatz is due to the area-law

nature of quantum entanglement entropy of ground states and shall not hold for highly excited or high-temperature states.

The MPS effectively expresses the ground states of quantum spin-chain models so that numerical methods can construct them more efficiently. We will use the time-evolving block decimation TEBD method [63] as described below to implement the imaginary-time evolution operator to obtain the ground states of the two considered spin-chain models and then use them to evaluate the generating (characteristic) function for the work statistics. Furthermore, when checking the fluctuation theorem, one must prepare the initial states as Gibbs states, which are beyond primitive MPS.

B. Time-evolving block decimation

Time-evolving block decimation (TEBD) provides an efficient way to simulate time evolution. We use the TEBD method to solve for the above MPS numerically, namely by acting the imaginary-time evolution operator $e^{-\tau H}$ on an initial state $|\psi_0\rangle$ to determine the ground state and by acting the real-time evolution operator e^{-iHt} to study the dynamics of the quantum lattice systems.

Denote the time-evolving state as $|\psi_t\rangle = e^{-itH}|\psi\rangle$ for an initial state $|\psi\rangle$ with a given Hamiltonian H. For simplicity, we consider only the Hamiltonians made of arbitrary single-site and two-site terms, i.e., with nearest-neighbor interactions, so that they can be decomposed as $H = \sum_{k=1}^{L} h_{k,k+1} = H_{\text{even}} + H_{\text{odd}}$, where $H_{\text{even}} \equiv \sum_{\text{even } k}^{L} h_{k,k+1}$, $H_{\text{odd}} \equiv \sum_{\text{odd } k}^{L} h_{k,k+1}$, and hence the commutator $[H_{\text{even}}, H_{\text{odd}}] \neq 0$. We then break the evolution operations e^{-itH} into a sequence of local gates using a Suzuki-Trotter expansion. For small enough δ, the Suzuki-Trotter expansion of order for e^{-itH} can be written as

$$\begin{aligned} e^{-itH} &= [e^{-i\delta H}]^{t/\delta} = [e^{-i\delta(H_{\text{even}}+H_{\text{odd}})}]^{t/\delta} \\ &\approx [f_p(e^{-i\delta H_{\text{even}}}, e^{-\delta H_{\text{odd}}})]^{t/\delta}, \end{aligned} \tag{32}$$

where $f_1 = (x, y) = xy$, $f_2 = (x, y) = x^{1/2}yx^{1/2}$ for first- and second-order expansions, respectively. If we expand to higher-order terms, the Trotter error will decrease. The evolution operators can be expressed as a product of two-body gates using the Suzuki-Trotter expansion. The simulation of evolution is achieved by updating the MPS by a sequential of alternating gate operations, i.e., alternating between $e^{-i\delta H_{\text{even}}}$ and $e^{-i\delta H_{\text{odd}}}$, as specified by Eq. (32). In this paper, we will implement this MPS-based TEBD method to evaluate the work characteristic function $G(u)$ for extracting average work done $\overline{W}$, and we will also evaluate the partition functions for extracting the free energies that appear on the right-hand side of the fluctuation theorem.

C. Thermal density matrix as MPO

As mentioned, the MPS is suitable for representing the ground states but not the highly excited states, such as high-temperature thermal states. This paper will mainly deal with the work statistics for ground states. On some occasions, we will also deal with thermal states, e.g., by checking the fluctuation theorem or the passivity of thermal states. A way to construct the thermal states based on MPS is the so-called algorithm of minimally entangled typical thermal states (METTS) [64], which adopts a Markov chain of product states to construct the thermal ensemble constrained by a detailed balancing relation.

Instead of adopting METTS, a more direct way of constructing a thermal state based on MPS is to represent the density operator $e^{-\beta H}$ by an MPO. The partition function for evaluating free energy is to take a trace of this MPO. To construct such an MPO, one first prepares an initial identity MPO of bond dimension $\chi_{\text{cut}} = 1$. The MPO for the thermal state is then obtained by acting with the operator $e^{-\beta H}$, which can be decomposed by TEBD and the Suzuki-Trotter expansion into a sequence of a product of two-body gates, as shown in Fig. 1(c). The partition function can be obtained by tracing out the two physical indices of the MPO $e^{-\beta H}$ as shown in Fig. 1(d). In Appendix B 1, we show the agreement on the work statistics obtained from METTS and MPO representation of thermal states. In the rest of the paper, we will adopt MPO to represent thermal states to proceed with the numerical calculations.

IV. NUMERICAL RESULTS FOR CHARACTERIZING THE QUANTUM PHASE TRANSITIONS

In this section, we will present our numerical results to demonstrate that the average work done by the sudden quench can be the order parameter for the quantum phase transitions. The quantum systems we consider include quantum spin-1/2 and spin-1 chains. The quantum phase transition considered for the spin-1/2 chain is the Landau-Ginzburg type due to spontaneous symmetry breaking. On the other hand, the ones for the spin-1 chain model are the topological phase transitions, which can only be characterized by nonlocal order parameters.

The average work done by sudden quench is given succinctly by Eq. (16) or extracted from the characteristic function provided by Eq. (15). In either case, we can implement the TEBD method based on MPS to evaluate it. Below, we will show the numerical results case by case.

A. Quantum spin-1/2 chain in magnetic field

We first consider the anisotropic Heisenberg XY spin-1/2 chain in a transverse magnetic field h_z and a longitudinal field h_x. Its Hamiltonian is given by

$$\begin{aligned} H = \sum_{k=1}^{n} \Bigg[&- \left(\frac{1+\gamma}{2} S_k^x S_{k+1}^x + \frac{1-\gamma}{2} S_k^y S_{k+1}^y \right) \\ &+ h_x S_k^x + h_z S_k^z \Bigg], \end{aligned} \tag{33}$$

where $S_k^{x,y,z}$ are the site spin-1/2 operators, and k labels the number of sites. When $\gamma = 1$, it reduces to the quantum Ising chain, and we will focus on the parameter range $0 \leqslant \gamma \leqslant 1$ and $h_x = 0$. The ground state of this model can be exactly solved and exhibits three phases of the Landau-Ginzburg-Wilson paradigm: the oscillatory phase (O), the ferromagnetic phase (F), and the paramagnetic phase (P) [65]. The ground state stays in the O phase for small h_z until $h_z = \frac{1}{2}\sqrt{1-\gamma^2}$ and then changes to the F phase as a crossover transition.

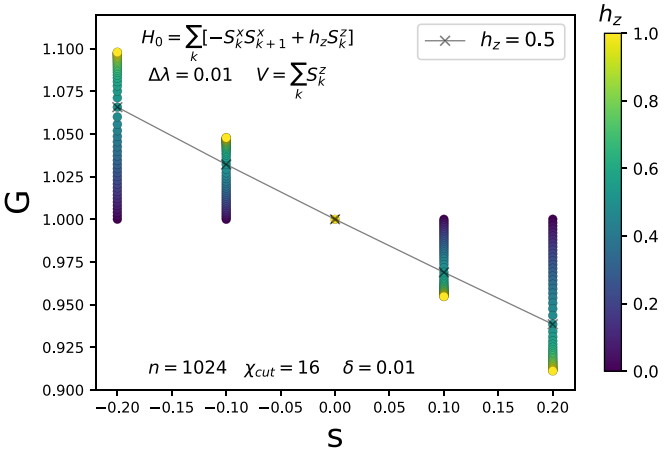

FIG. 2. Work characteristic function $G(-is)$ under a sudden quench process implemented by Hamiltonian $H = H_0 + \Delta\lambda\, V$ with $\Delta\lambda = 0.01$ with H_0 of an $n = 1024$ quantum Ising chain, i.e., (33) of $\gamma = 1$, $h_x = 0$, $h_z \in [0, 2]$, and $V = \sum_k S_k^z$. The results are obtained by the MPS-based TEBD method via the first-order Trotter expansions for $\delta = 0.01$ with bond dimension $\chi_{\rm cut} = 16$. We show the results only for five values of s but can connect them into a line by Lagrange interpolation. Each color represents one particular choice of h_z, with their values indicated by the color sidebar. The Lagrange interpolating lines at critical points are shown explicitly for $h_z = 0.5$. The slope of an interpolating line corresponds to the average work done $\overline{W}$, which is mostly negative.

Further increasing h_z up to $h_z = 0.5$, the ground state will change to P phase, which is a second-order quantum phase transition in the thermodynamic limit with $\langle S^x \rangle$ as the order parameter, i.e., $\langle S^x \rangle$ is nonzero in F (or O if $\gamma = 0$) phase but zero in P phase. Below, we will consider the phase transition between the ferromagnetic and paramagnetic phases.

Here, we apply the MPS-based TEBD method to calculate the characteristic function $G(u)$ of Eq. (10) for this spin chain model with $\gamma = 1$ and $h_x = 0$ at zero temperature but varying the transverse field h_z. We aim to check if the work done $\overline{W}$ can be used as an order parameter for the quantum phase transition, i.e., from F (or O if $\gamma = 0$) phase to P phase. For simplicity, we consider the sudden quench process implemented by the Hamiltonian of Eqs. (11) and (12) with a chosen jump of the coupling constant, i.e., $\Delta\lambda = 0.01$. The results are shown in Figs. 2 and 3.

Figure 2 shows the characteristic function $G(-is)$ of an $n = 1024$ Ising chain for $s \in [-0.2, 0.2]$ with $\gamma = 1$ and $h_x = 0$ at various values of h_z in the initial Hamiltonian H_0. For simplicity, we pick five values of s but vary h_z continuously, with its value indicated by the color bar attached aside. In particular, the five points belonging to $h_z = 0.5$ are denoted by the crosses and joined into a line by Lagrange interpolation. We see that the slope of this line is negative, which implies that the average work done, $\overline{W} = \lim_{s\to 0} \frac{\partial G(-is)}{\partial s}$, is negative. For other values of h_z in the initial Hamiltonian H_0, we can see that the slope of the line connected by the five points of the same h_z starts with a positive value for $h_z = 0$, then gradually turns negative as h_z increases, and finally converges to a constant negative value.

The above results and further related calculations can be translated into phase diagrams as shown in Fig. 3 for the quantum phase transition from the F (or O) phase to the P phase. These phase diagrams are characterized by the entanglement entropy S, the average work done, $\overline{W}$, and its associated higher moments and cumulants, under a sudden quench process with $V = \sum_k S_k^z$ and $\Delta\lambda = 0.01$. We see that S has a sharp peak near $h_z = 0.5$, which implies a stronger correlation near the

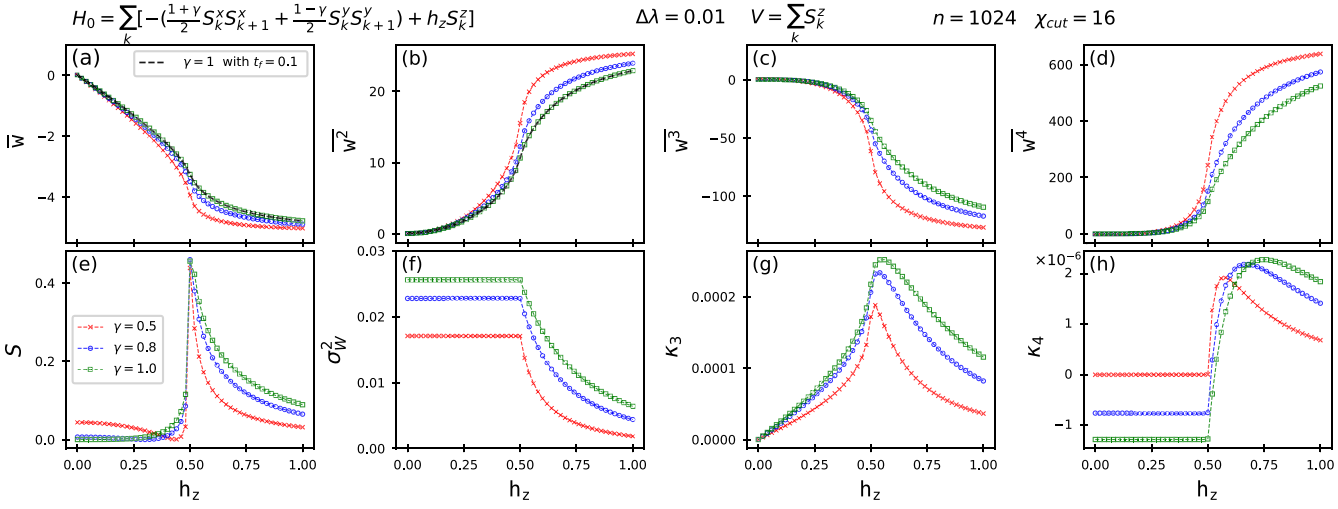

FIG. 3. Moments and cumulants of work done by sudden quench with $V = \sum_k S_k^z$ and $\Delta\lambda = 0.01$ on the quantum Heisenberg XY Ising chain of size $n = 1024$ as a function of the transverse field h_z at zero temperature for $\gamma = 0.5$ (red crosses), 0.8 (blue circles), and 1.0 (green squares). For comparison, the entanglement entropy S is also shown. They are listed as follows: (a) $\overline{W}$, (b) $\overline{W^2}$, (c) $\overline{W^3}$, (d) $\overline{W^4}$, (e) S, (f) σ_W^2, (g) κ_3, and (h) κ^4. The plots are obtained by the TEBD method with the parameters $\chi_{\rm cut} = 16$ and $\delta = 0.01$, and $\overline{W^n}$ are obtained using Eq. (16) by the MPO method. As expected, the higher moments or cumulants yield a sharper change near the critical point so that the work statistics can indicate the quantum phase transitions in the Ising-like spin chains. To go beyond sudden quench and for comparison, we also extract $\overline{W}$ and $\overline{W^2}$ (black dashed lines) from the characteristic function Eq. (10) for the nonsudden quench process with $t_f = 0.1$.

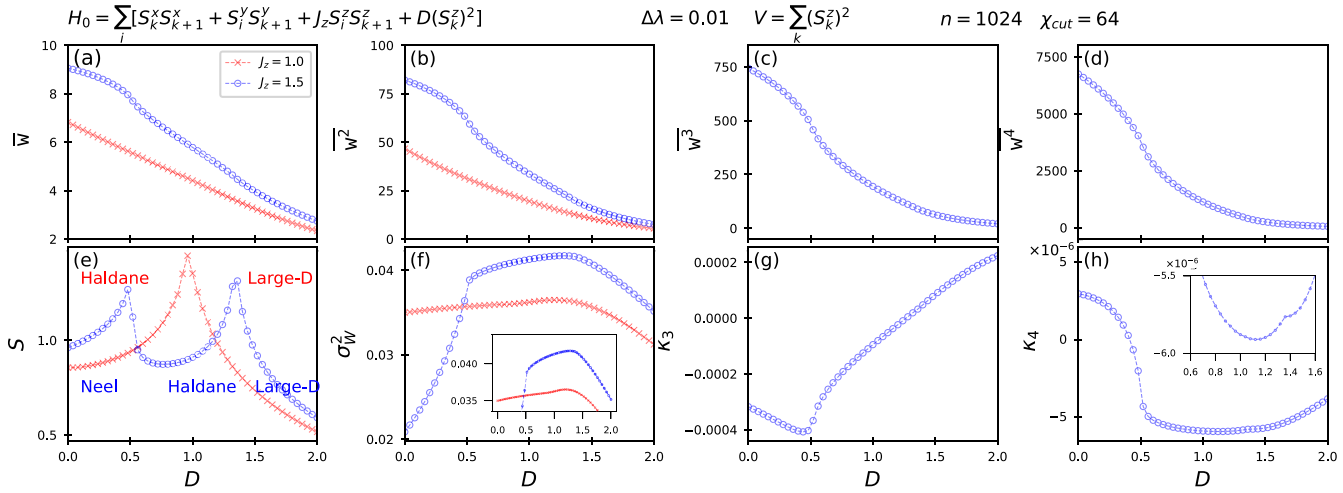

FIG. 4. Moments and cumulants of work done by sudden quench with $V = \sum_k (S_k^z)^2$ and $\Delta\lambda = 0.01$ on a quantum Heisenberg XXZ Haldane chain of size $n = 1024$ as a function of the coupling parameter D at zero temperature for $J_Z = 1.0$ (red crosses) and 1.5 (blue circles). For comparison, the entanglement entropy S is also shown. The listing order for $\overline{W^{m=1,\ldots,4}}$, σ_W^2, $\kappa_{\ell=3,4}$, and S, the subfigure captions, and the numerical implementing methods are the same as in Fig. 3. The quantum critical points are indicated by the sharper behavior of S, and they are at (i) $(J_z, D) = (1.5, 0.48)$, (ii) $(J_z, D) = (1.5, 1.34)$, and (iii) $(J_z, D) = (1.0, 1.0)$. Note that (i) is the transition point from the ordered phase to the topological phase, but (ii) and (iii) are the purely topological ones without any order parameter, and they should be more difficult to detect. For (i), $\overline{W^{m=1,\ldots,4}}$ show very mild behavior, but cumulants show sharper changes as the order of cumulants goes higher. However, for (ii) and (iii), only σ_W^2 and κ_4 show mild crossover [see the enlargement insets in the subfigures (f) and (h)], and all the other moments/cumulants in this figure show no obvious changes. Overall, we can conclude that the work statistics can barely capture the purely topological phase transitions. The plots are obtained by the TEBD method with the parameters $\chi_{\rm cut} = 64$ and $\delta = 0.01$.

critical point at $h_z = 0.5$. Similarly, the work statistics denoted by $\overline{W}$ and the higher moments and cumulants also show shaper changes near $h_z = 0.5$. As expected, the higher moments and cumulants show sharper changes at the critical point. This implies that the work statistics can indicate the phase transitions. Interestingly, the cumulants of even orders show a level-off for the F (or O) phase with $h_z \leqslant 0.5$, and similar behavior for σ_W^2 has been observed earlier, obtained by the exact solution of Ising chains [66]. This constancy could be associated with some underlying symmetry. However, the quantities $\langle V^n \rangle$ with $V = \sum_k S_k^z$, related to the cumulants of work, are different from the order parameter $\langle \sum_k S_k^x \rangle$ for the transition from the F (or O) phase to the P phase.

In addition, in Appendix B 2, we give a consistency check to show in Fig. 13 that the above numerical results of $\overline{W}$ and $\overline{W^2}$ obtained from either Eq. (7) or Eq. (16) agree.

B. Anisotropic quantum spin-1 chain

To show that our proposal can also work for the quantum phase transitions of the non-Landau-Ginzburg-Wilson type, we consider a particular model of such type, namely the anisotropic quantum XXZ spin-1 chain, described by the following Hamiltonian:

$$H = \sum_{k=1}^{n} \left[S_k^x S_{k+1}^x + S_k^y S_{k+1}^y + J_z S_k^z S_{k+1}^z + D\left(S_k^z\right)^2 \right], \qquad (34)$$

where $S_k^{x,y,z}$ are the site spin-1 operators, and the parameter D denotes the uniaxial anisotropy. When $J_z = 1$, it reduces to the so-called Haldane chain. The ground-state phase diagram of this model consists of six different phases [67,68]. Here, we focus on phase transitions among three phases: the large-D phase, the Néel phase, and the Haldane phase characterized by nonzero string-order parameters. At large D, the model is in a trivial insulator phase. Namely, the ideal large-D phase is $|000\cdots\rangle$. On the other hand, the ideal Néel phase is $|1, -1, 1, -1\cdots\rangle$ or $|-1, 1, -1, 1\cdots\rangle$ with spontaneous nonzero expectation values of the staggered magnetization.

The Haldane phase is one of the symmetry-protected topological (SPT) phases. The ground states of such phases have nontrivial patterns of quantum entanglement. They cannot continuously connect to trivial product states without closing the gap or breaking the protecting symmetry. Thus, the SPT phases preserve the global symmetry of the Hamiltonian so that some spontaneous symmetry-breaking local order parameters cannot characterize the transition from the SPT-nontrivial phase to the SPT-trivial one. This is in contrast to the cases of the Landau-Ginzburg type. Instead, the topological phases, such as the Haldane phase, are characterized by fractionalized edge excitations, which some nonlocal order parameters, such as the expectation value of some stringlike operator, can measure.

As before, we can characterize the quantum phase transitions of this model by entanglement entropy S, the average work done $\overline{W}$ and its higher moments/cumulants by a sudden quench with $V = \sum_k (S_k^z)^2$ and $\Delta\lambda = 0.01$, and by the associated higher moments and cumulants. The results are shown in Fig. 4, which are again obtained numerically using the MPS-based TEBD method. We see that the entanglement entropy S shows the peaks around three quantum critical points, which are at (i) $(J_z, D) = (1.5, 0.48)$, (ii) $(J_z, D) = (1.5, 1.34)$, and (iii) $(J_z, D) = (1.0, 1.0)$. The critical point (i) is the transition

point from the ordered Néel phase to the topological Haldane phase and is partly with local order parameters. On the other hand, the critical points (ii) and (iii) are from the Haldane phase to the large D phase, and no local parameter exists to characterize it. Therefore, these transitions are purely topological types and should be more difficult to detect. Indeed, this is what we see from Fig. 4. For (i), $\overline{W^{m=1,\ldots,4}}$ show very mild behavior, but cumulants show shaper changes as the order of cumulants goes higher. However, for (ii) and (iii), only σ_W^2 shows a mild crossover, and all the other moments/cumulants in this figure show no obvious changes. It is strange why the higher cumulants do not show sharper behavior for critical points (ii) and (iii). This could be due to the need for a higher bond dimension to capture the behavior of higher cumulants. Overall, we can conclude that the work statistics can barely capture the purely topological phase transitions, because work statistics involve all multipoint correlations, and they could be used as some nonlocal order parameter. Thus, we expect the higher moments and cumulants of the work statistics to display shaper behavior around the topological phase transitions, although it is quite computationally costly to obtain higher moments and cumulants due to the need for large bond dimensions.

Also, in Appendix B 2, we give a consistency check to show in Fig. 14 that the above numerical results of $\overline{W}$ obtained from either Eq. (7) or Eq. (16) agree. However, the $\overline{W^2}$ obtained from either Eq. (7) or Eq. (16) cannot match well. The larger bound dimension χ_{cut} might improve the physical properties near critical points.

V. BENCHMARKING THE REAL-TIME EVOLVING METHODS BY JARZYNSKI'S EQUALITY

We now adopt the Jarzynski equality of Eq. (9) dictated by the real-time correlator expression of the work characteristic function $G(i\beta;t_f)|_{\beta=1}$, i.e., Eq. (10), to benchmark the numerical accuracy of the real-time evolution of two quantum spin chain models considered above. The numerical error mainly comes from evaluating $G(i\beta;t_f)$ and accumulates as t_f grows. For the small-size cases, we can use either the exact diagonalization (ED) method or the MPS-based TEBD method. For large-size cases, we can only use the TEBD method. As before, the nonequilibrium process is implemented by the Hamiltonian of Eq. (11), and here we adopt the linear profile of coupling constant, i.e., $\lambda(t)=t$. The results for the small-size cases are shown in Fig. 5 for (a) an $n=10$ Ising chain of fixed $h_{x,z}$ and with $V=\sum_i S_i^z$, and (b) an $n=6$ Haldane chain of fixed $D=2$ and with $V=\sum_i (S_i^z)^2$. Figure 5 shows that as t_f increases, the curve of $G(i\beta;t_f)|_{\beta=1}$ of the Ising chain increases; on the other hand, the curve in the Haldane chain decreases.

Next, we use the Jarzynski equality to characterize the numerical error of real-time evolution and benchmark the corresponding numerical methods. This can be quantified by the ratio $R(t_f)=\frac{G(i\beta;t_f)}{Z(t_f)/Z(0)}|_{\beta=1}$ defined in Eq. (14), which is the ratio between either side of the Jarzynski equality. If there is no numerical error, the Jarzynski equality is obeyed so that $R=1$. Otherwise, the $|1-R|$ size can characterize the numerical error.

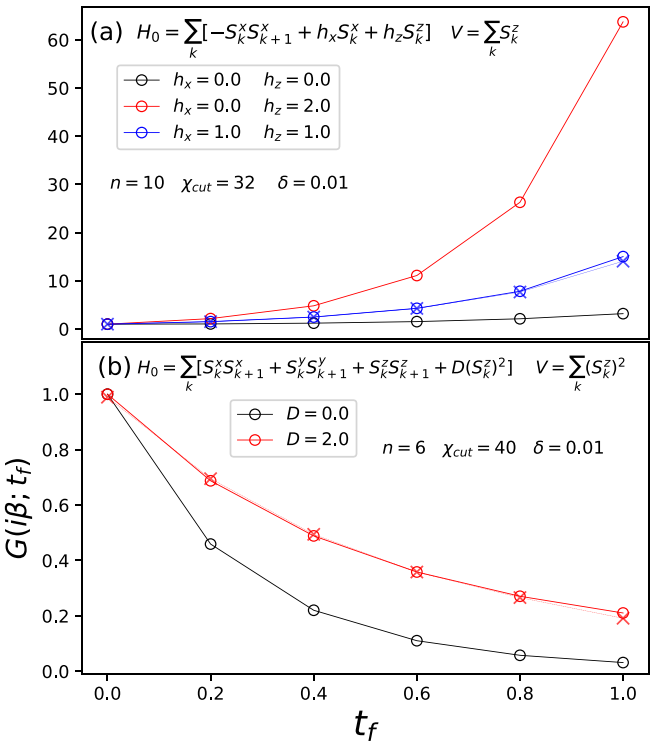

FIG. 5. Work characteristic function $G(i\beta;t_f)|_{\beta=1}$ implemented by Hamiltonian $H=H_0+\lambda(t)V$ with $\lambda(t)=t$, for (a) an $n=10$ Ising chain and (b) an $n=6$ Haldane chain, with their H_0 and V shown on the corresponding subfigures. We obtain the results by using the ED method (circles) and the MPS-based TEBD method (crosses) with the parameters $\chi_{\text{cut}}=40$ and $\delta=0.01$. In some cases, the results from both ED and MPS agree. Note that $G(i\beta;t_f)|_{\beta=1}$ increases with time for (a) but decreases for (b).

We can evaluate the partition function ratio $\frac{Z(t_f)}{Z(0)}|_{\beta=1}$ by ED and TEBD methods. As expected, both methods can be accurate for such a nondynamical quantity. Combined with the previous results for $G(i\beta;t_f)|_{\beta=1}$, we can evaluate R. The results for small-size quantum chains are shown in Fig. 6 with subfigure (a) for an $n=10$ quantum Ising chain and subfigure (b) for an $n=6$ Haldane chain. We see that R remains 1 for the ED method. However, for the MPS-based method, the numerical errors escalate around some critical moment, i.e., $(t_f)_c=0.7$, as shown in Figs. 6(a) and 6(b). Moreover, we also evaluate and show the ratio of the partition functions obtained by ED and MPS-based methods, i.e., $\frac{Z(t_f)}{Z(0)}|_{\text{MPS}}/\frac{Z(t_f)}{Z(0)}|_{\text{ED}}$ [black triangles in Figs. 6(a) and 6(b)]. In Fig. 6(c), we show the dependence of the resultant $R(t_f)$ of the $n=6$ Haldane chain on MPS's bond dimension χ_{cut}. The larger χ_{cut} yields better results, as expected. In this case, $\chi_{\text{cut}}\geqslant 40$ is needed to arrive at an accurate $R=1$ result for $t_f\leqslant 1$.

When the quantum spin chain size becomes large, the ED method is unavailable, and we can only use the MPS-based method to evaluate R. For comparison, we evaluate the benchmarking factor R for an $n=100$ Ising chain with the same H_0, V, χ_{cut}, and δ as in the $n=10$ case of Fig. 6(a). The results of $G(i\beta;t_f)|_{\beta=1}$, $R(t_f)$, and $\frac{Z(t_f)}{Z(0)}|_{\beta=1}$ are shown in Fig. 7. As we can see, $G(i\beta;t_f)|_{\beta=1}$ grows exponentially

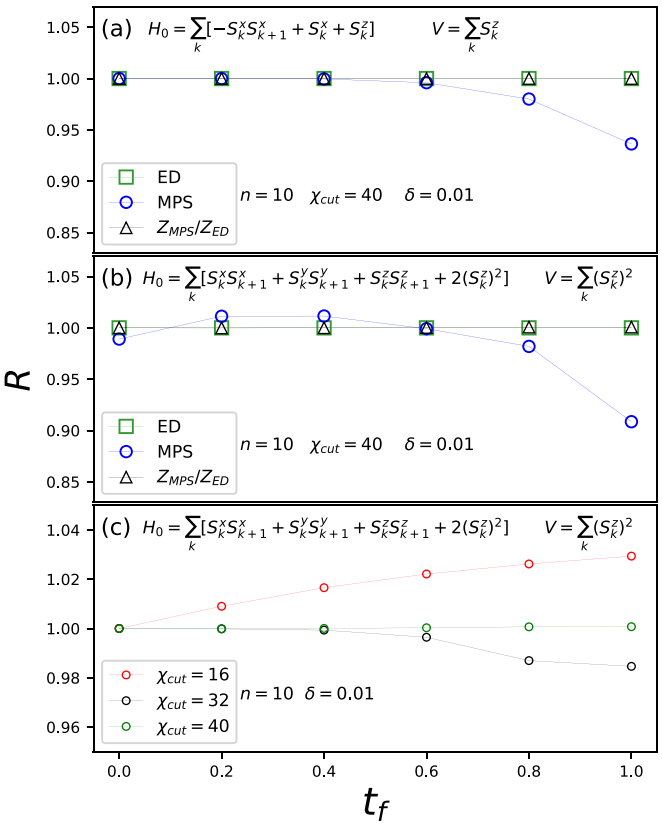

FIG. 6. Benchmarking the ED and TEBD methods by the ratio $R(t_f) = \frac{G(i\beta;t_f)}{Z(t_f)/Z(0)}|_{\beta=1}$ from the Jarzynski equality for subfigure (a) an $n = 10$ Ising chain with $h_x = h_z = 1$ and $V = \sum_k S_k^z$, and subfigure (b) an $n = 6$ Haldane chain with $D = 2$ and $V = \sum_k (S_k^z)^2$. In subfigure (c) we show the dependence of the resultant $R(t_f)$ of an $n = 6$ Haldane chain on the bond dimension χ_{cut} of MPS. As expected, larger χ_{cut} yields better results. The results from ED are indicated by squares, and from TEBD they are indicated by circles. In addition, we also show the ratio $\frac{Z(t_f)}{Z(0)}|_{\text{MPS}}/\frac{Z(t_f)}{Z(0)}|_{\text{ED}}$ [triangles in subfigures (a) and (b)] to demonstrate the accuracy of TEBD in evaluating the partition functions. In all the above, the coupling constant has a linear profile, i.e., $\lambda(t) = t$. If there is no numerical error, $R = 1$, and the deviation benchmarks the real-time numerical errors. For ED, we see that R remains equal to 1. On the other hand, for MPS, we see that the real-time numerical errors start to escalate around $t_f = 0.7$. However, the ratio of partition functions remains accurate.

with t_f, which should cause large numerical errors. Indeed, the real-time numerical errors characterized by $|1 - R|$ start to escalate around the critical moment $(t_f)_c = 0.13$. This is far shorter than $(t_f)_c = 0.7$ of the $n = 10$ case, as we expect that the numerical errors accumulate more quickly for systems of larger sizes.

VI. NUMERICAL RESULTS FOR EXAMINING THE PASSIVITY OF THERMAL/GROUND STATES

We can now consider the passivity of a given initial state undergoing a (cyclic) impulse process. Two natural candidate categories are thermal or ground states. The passivity of (relativistic) thermal states was shown to be ensured [45–47]. For the thermal states of the nonrelativistic systems, such as

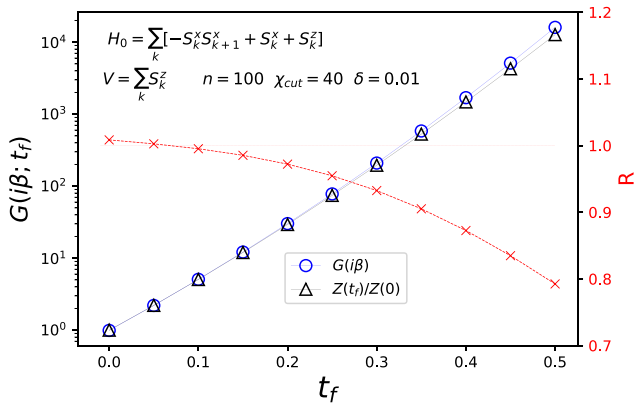

FIG. 7. Benchmarking the numerical accuracy with the Jarzynski equality for an $n = 100$ Ising chain with the same H_0, V, χ_{cut}, and δ as in Fig. 6(a). The results for $G(i\beta;t_f)|_{\beta=1}$, $R(t_f)$, and $\frac{Z(t_f)}{Z(0)}|_{\beta=1}$ are denoted by blue circles, red crosses, and black triangles, respectively. Due to the large size, ED is unavailable, and the results are obtained by the TEBD method. We see that the real-time numerical errors start to escalate around $t_f = 0.13$, which is far shorter than the $n = 10$ case, as expected. However, the ratio of partition functions remains accurate as in the $n = 10$ case.

the quantum spin chains, as argued in Eq. (22), the passivity should be guaranteed by the fluctuation theorem, i.e., the second law of thermodynamics. Here, we demonstrate that this is the case for the $n = 10$ Ising chain. The result is shown in Fig. 8, from which we see that the average work done per site $\overline{w}^{\text{impluse}} = -w_{\text{ext}}^{\text{impulse}}$ for the thermal state at $\beta = 1$ is always positive for various V and λ.

We now turn to the issue of passivity for the ground states under the cyclic impulse processes. As shown in Sec. II D, the passivity of ground states is guaranteed to be passive under the Hermitian action, i.e., $V^\dagger = V$ by the variational principle. This is because the average work extraction from a cyclic process can be understood as the energy difference between

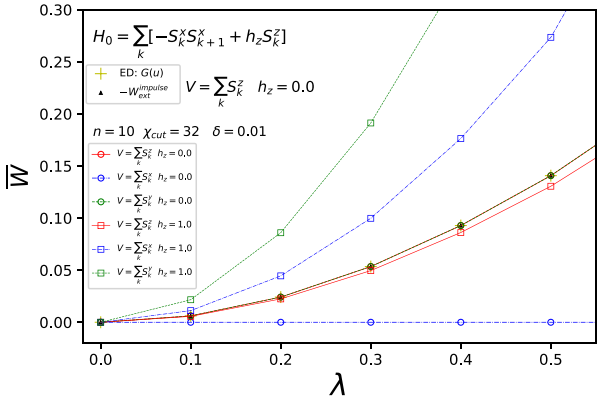

FIG. 8. Demonstration of passivity of thermal states in an $n = 10$ quantum Ising chain under an impulse process implemented by the Hamiltonian of Eqs. (11) and (13) with H_0 of Eq. (33) with $h_x = h_z = 0$ and with $V = \sum_k S_k^x$, $\sum_k S_k^y$, or $\sum_k S_k^z$. The resultant average work done per site $\overline{w}^{\text{impulse}}$ for $\beta = 1$ is obtained by ED and TEBD. Its positiveness for all considered V's and $\lambda \in [0, 0.5]$ demonstrates the passivity of thermal states as pointed out in Eq. (22).

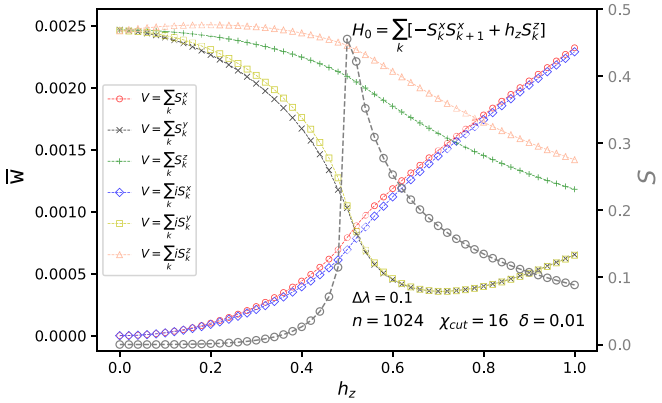

FIG. 9. Plot of $\overline{w}^{\text{impulse}}$ to show the passivity of ground states of an $n = 1024$ quantum Ising chain with $h_x = 0$ but varying $h_z \in [0, 1]$ under an impulse process implemented by the Hamiltonian of Eqs. (11) and (13) with $\lambda = 0.1$ and Hermitian actions $V = \sum_k S_k^x$ (red circles), $\sum_k S_k^y$ (black cross), $\sum_k S_k^z$ (green cross), and non-Hermitian actions $V = \sum_k iS_k^x$ (blue diamonds), $\sum_k iS_k^y$ (yellow square), $\sum_k iS_k^z$ (pink triangles). Again, we see that $\overline{W}^{\text{impulse}}$ can also indicate a quantum phase transition by mild crossover behaviors when compared with the phase diagram of the entanglement entropy of the initial state (gray circle).

the ground state and the excited state driven by V. It is always negative as the variational principle guarantees. On the other hand, there is no such simple interpretation for the average work extraction if the action V is non-Hermitian, i.e., one cannot apply the variational principle to check the passivity of ground states. For the latter cases, it is then interesting to examine the passivity by evaluating average work extraction numerically.

As a startup, we numerically examine the passivity of ground states for various Hermitian or non-Hermitian actions but small λ, i.e., $\lambda = 0.1$. In Fig. 9, We plot the average work done per site $\overline{w}^{\text{impluse}} = -w_{\text{ext}}^{\text{impulse}}$ as a function of h_z, which labels the ground states of the Ising-like chain under various Hermitian and non-Hermitian actions. A similar result for Haldane-like chains is also given in Fig. 16 of Appendix C. To obtain these results, we first evaluate $G(-is)$ by the MPS-TEBD method, and from that we extract $\overline{w}^{\text{impluse}} = -w_{\text{ext}}^{\text{impulse}}$ from $G(-is)$. The ground states considered are all passive under the various Hermitian and non-Hermitian actions described in Fig. 9. This is a consistency check for our numerical method with the discussion in Sec. II D for examining the passivity of ground states of Ising-like chains.

By exploiting the numerical method's power in checking the ground states' passivity, we now consider the cases with quite an extensive range of $\lambda \in [-10, 10]$ for both Hermitian and non-Hermitian actions. The results for the Ising-like chains are shown in Fig. 10, and similar results for the Haldane-like chains and the more general non-Hermitian actions in the Ising-like chains are shown in Figs. 17 and 15 of Appendix C, respectively. Since the ones shown in Appendix C resemble those in Fig. 10, we will not discuss them in the main text. The top row of Fig. 10 shows the average work done per site on the ground states labeled by the values of $h_z \in [0, 1]$ for the Hermitian actions $V = \sum_k S_k^{x,y,z}$, and the bottom row shows the results for the non-Hermitian actions $V = i \sum_k S_k^{x,y,z}$. For the Hermitian cases, we see a quite interesting feature that $\overline{W}^{\text{impulse}}$ is periodic with respect

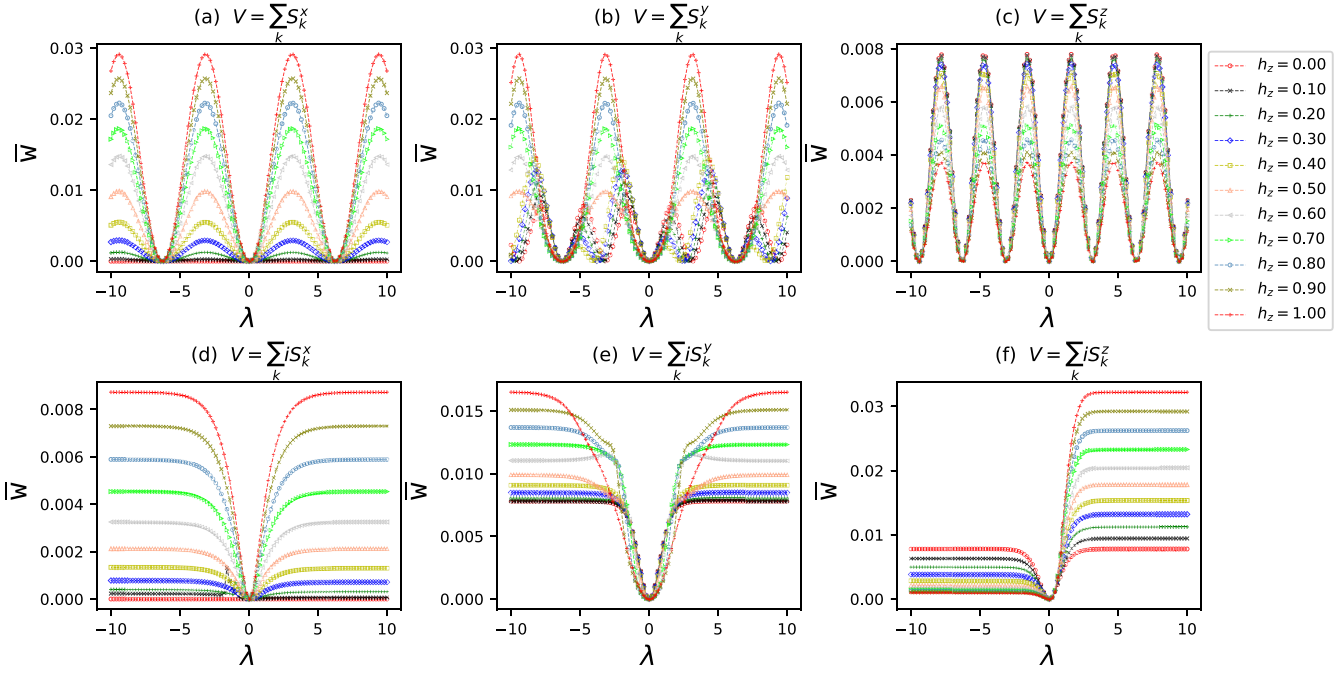

FIG. 10. Plot of $\overline{w}^{\text{impulse}}$ to show the passivity of ground states and its pattern as a function of the coupling λ of an $n = 1024$ quantum Ising chain. We fix $h_x = 0$ but vary $h_z \in [0, 1]$ to obtain various ground states, and we also vary $\lambda \in [-10, 10]$ under an impulse process implemented by the Hamiltonian of Eqs. (11) and (13) with the Hermitian actions (a) $V = \sum_k S_k^x$, (b) $V = \sum_k S_k^y$, and (c) $V = \sum_k S_k^z$ in the top row, and the non-Hermitian actions (d) $V = i \sum_k S_k^x$, (e) $V = i \sum_k S_k^y$, and (f) $V = i \sum_k S_k^z$ in the bottom row.

to the coupling λ with the period equal to 2π or π. This periodic behavior has been discussed in Sec. II D due to the peculiar feature of the impulse process. We will not see such behavior for the cyclic process with a finite time duration. For the non-Hermitian case, we first see that all the ground states considered are passive as in the Hermitian cases. However, $\overline{W}^{\text{impulse}}$ is no longer periodic with respect to λ but levels off as λ becomes large. In both cases, the average work done is bounded no matter how large the coupling λ is. Again, this is due to the zero time duration of the impulse process, so the average work done is limited to such a tiny time duration. However, it is unclear why the passivity remains intact for non-Hermitian action, especially without the guarantee by the variational principle. This issue deserves future study to explore.

VII. CONCLUSIONS

In this paper, we apply the numerical method for real-time evolution, such as exact diagonalization (ED) and MPS-based TEBD, to quantum spin lattice models to study the work statistics. With the power of MPS formalism, we can evaluate the chains up to 1024 sites, which can effectively suppress the finite-size effect. We focus on three aspects: (i) we study the behaviors of the moments and cumulants of the work statistics near the quantum phase transitions and examine their capability to indicate quantum critical points; our results up to the fourth cumulant show that the work statistics can detect the quantum phase transitions characterized with local order parameters, but just barely for the topological phase transitions; (ii) we propose to adopt the Jarzynski equality as the benchmark for the accuracy of the numerical real-time evolution methods; and (iii) we examine the passivity of thermal states and ground states of quantum spin chains under some cyclic impulse processes. Our numerical results show that all the ground states are passive under both Hermitian and non-Hermitian actions considered in this work. Although the variational principle ensures the passivity of ground states under Hermitian actions, it is not the case for non-Hermitian actions. It is interesting to explore the reason for the passivity of ground states under non-Hermitian action seen in this paper, and also the possibility of active ground states by more general actions. Once the active ground states exist, we may adopt them to implement the quantum engine naturally to extract quantum work in the cyclic processes.

The quantum spin lattice with nearest-neighbor interactions can be the natural system for performing quantum simulation and can serve as accurate tests for work statistics such as fluctuation theorem. Due to the statistical nature of quantum work, it has remained quite mysterious since its proposal decades ago. With our demonstration of numerical studies for realistic many-body systems, one can explore more different perspectives of work statistics. For example, when using pure states as the initial states for the work statistics, it may require a more subtle treatment than the two-point measurements to preserve the quantum coherence and explore its role in the fluctuation theorem. We hope to adopt a real-time evolution method, such as the MPS-based one, to investigate the role of pure states in some specific quantum tasks.

ACKNOWLEDGMENTS

We thank Masahiro Hotta and Jhh-Jing (Arthur) Hong for their helpful discussions. F.-L.L. is supported by the National Science and Technology Council through Grant No. 112-2112-M-003-006-MY3. C.-Y.H. is supported by the National Science and Technology Council through Grant No. 112-2112-M-029 -006.

APPENDIX A: TENTATIVE STUDY OF THE DENSITY OF STATE IN EQ. (21)

In Sec. II C, we argue why the average work done $\overline{W}$ can be used as the local order parameter for a quantum phase transition. As $\overline{W}$ can be expressed in (21) as the average over the eigenenergies of the final Hamiltonian, it will have a sudden change when crossing the quantum critical point because the probabilities of states $p(f)$ in (21) for the gapped and the gapless phases have rather different behaviors at low energy of an extensive system.

Therefore, it is interesting to calculate $p(f)$ and examine the behaviors of the gapped and gapless phases of an extensive spin chain. Unfortunately, the MPS-based method used for the main calculations of the long spin chain cannot be applied to the excited states. We can only study $p(f)$ tentatively by using the ED method for the short spin chains. In this case, we will miss the ground-state degeneracy for the gapless phases due to the sizable finite-size effect. Despite that, we still present the ED results of $p(f)$ as a function of the eigenenergy E_f of the $n = 10$ quantum spin chains with $h_z = 0.4, 0.5, 1.0$ under a sudden quench process with $V = \sum_k S_k^z$ and $\Delta\lambda = 0.1$. The result is shown in Fig. 11. As expected, due to the large finite-size effect for $n = 10$, it is hard to see the effect of ground-

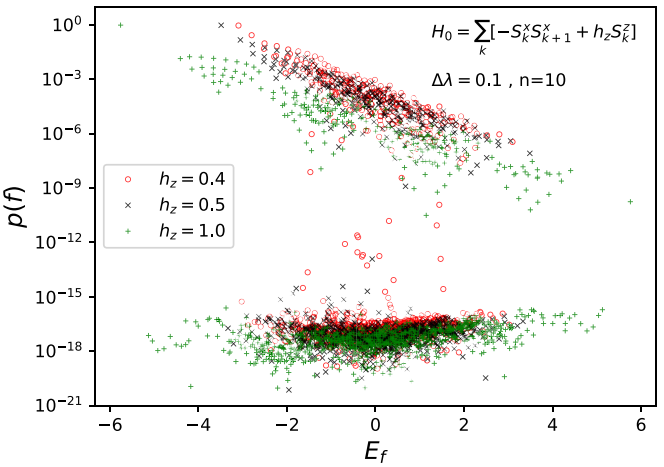

FIG. 11. The ED results of weight $p(f)$ from Eq. (21) are plotted as a function of the eigenenergy E_f of the Hamiltonian $H_+ = H_0 + \Delta\lambda V$ for the $n = 10$ quantum Ising chains with $h_z = 0.4, 0.5, 1.0$ under a sudden quench process with $V = \sum_k S_k^z$ and $\Delta\lambda = 0.1$. We can see that the $p(f)$'s for $h_z = 0.5$ (black crosses) and $h_z = 0.4$ (red circles) have a more focused energy spectrum than the one for $h_z = 1.0$ (green pluses). Note that for $h_z = 0.5$ ($h_z = 0.4$), the initial (final) Hamiltonian is in the critical phase because $\Delta\lambda = 0.1$. Thus, the more focused energy spectrum for these two cases implies a tendency for the effect of ground-state degeneracy.

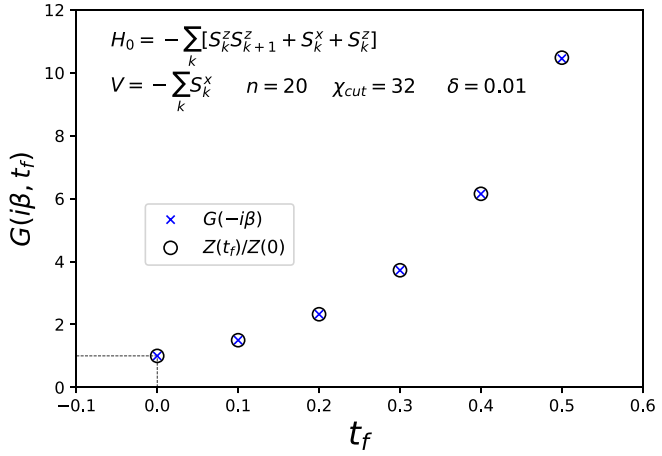

FIG. 12. Numerical agreement of the results for the Jarzynski equality. We evaluate the work characteristic function $G(i\beta; t_f)|_{\beta=1}$ (crosses) and the ratio of partition functions $\frac{Z(t_f)}{Z(0)}|_{\beta=1}$ (circles) for an $n = 20$ quantum Ising chain by TEBD and MPO of $\chi_{\text{cut}} = 32$ and $\delta = 0.01$ to represent the thermal states. The result shows that the Jarzynski equality holds and justifies using MPO for constructing the thermal states. After comparison, we also find that our results numerically agree with those from the ensemble of 10 000 METTS, as shown in Fig. 4 in Ref. [28].

state degeneracy on $p(f)$ for either $h_z = 0.5$ (black crosses) with the initial Hamiltonian in the critical phase, or $h_z = 0.4$ (red circles) with the final Hamiltonian in the critical phase as $\Delta\lambda = 0.1$. However, we can see that the $p(f)$'s for these two cases are more focused than the one with $h_z = 1.0$ (green pluses). This implies a tendency for the effect of ground-state degeneracy.

APPENDIX B: TWO NUMERICAL CONSISTENCY CHECKS

In this Appendix, we demonstrate two consistency checks relating to work statistics numerically.

1. Equivalence between thermal representations by MPO and METTS

We present in Fig. 12 our numerical results of the work characteristic function $G(i\beta; t_f)|_{\beta=1}$ and the ratio of partition functions $\frac{Z(t_f)}{Z(0)}|_{\beta=1}$ for checking the fluctuation theorem of an $n = 20$ quantum Ising chain by TEBD and the MPO representation for the thermal states. Our results agree numerically with those from METTS, shown in Fig. 4 of Ref. [28]. This can justify our usage of MPO representation of thermal states for examining the passivity of thermal states, as shown in Fig. 8.

2. Equivalence between average works obtained from Eq. (10) or from Eq. (16)

There are two ways to obtain the average work done by a sudden quench process. The first one is to extract it from the work characteristic function $G(u)$ of Eq. (10) by using Eq. (7). The second one calculates it by evaluating the vacuum

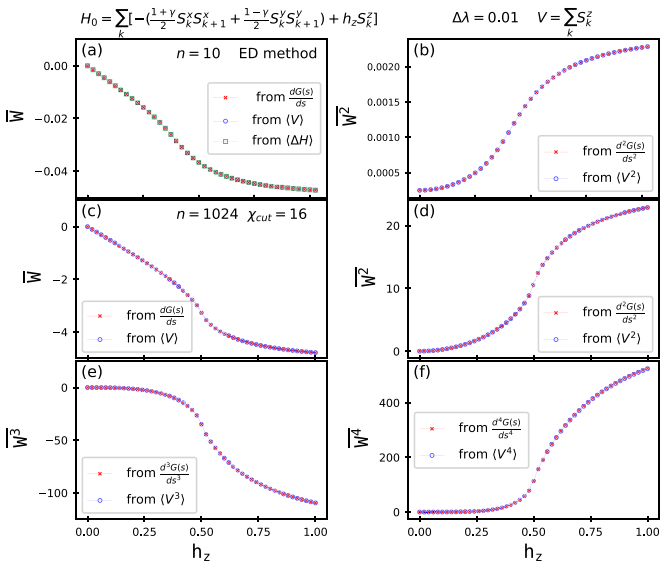

FIG. 13. Agreement of $\overline{W^m}$ of $m = 1, 2, 3, 4$ obtained from either the characteristic function $G(-is)$ of Eq. (10) (red crosses) or from the VEV of V^m (blue circles) for the transverse quantum Ising chains under sudden quench process with $V = \sum_k S_k^z$ and $\Delta\lambda = 0.01$. In (a) and (b), the result for $n = 10$ chains is obtained by the ED method, and (a) also shows the result from the VEV of the Hamiltonian offset by Eq. (16) (green squares). In (c), (d), (e), and (f), the results for $n = 1024$ chains are calculated by the MPS-based method.

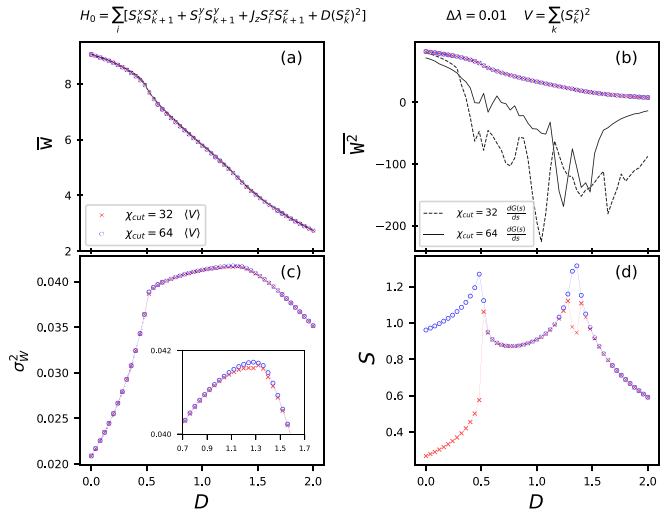

FIG. 14. Examining the agreement of (a) $\overline{W}$, (b) $\overline{W^2}$, and (c) σ_W^2 for an $n = 1024$ Haldane (XXZ) chain with various coupling D in the initial Hamiltonian H_0 of size $n = 1024$ under a sudden quench process with $V = \sum_k (S_k^z)^2$ and $\Delta\lambda = 0.01$. These results are obtained from the characteristic function $G(-is)$ (black dashed line for $\chi_{\text{cut}} = 32$ or solid line for $\chi_{\text{cut}} = 64$) or from the VEV of V^m (red crosses for $\chi_{\text{cut}} = 64$ or blue circles for $\chi_{\text{cut}} = 64$). We see that the results from both methods match well for (a) and (c) but not for (b). We thus evaluate entanglement entropy S in (d) to show the relevance of increasing the bond dimension χ_{cut} in improving the accuracy, which could also be the reason for the mismatch in (b).

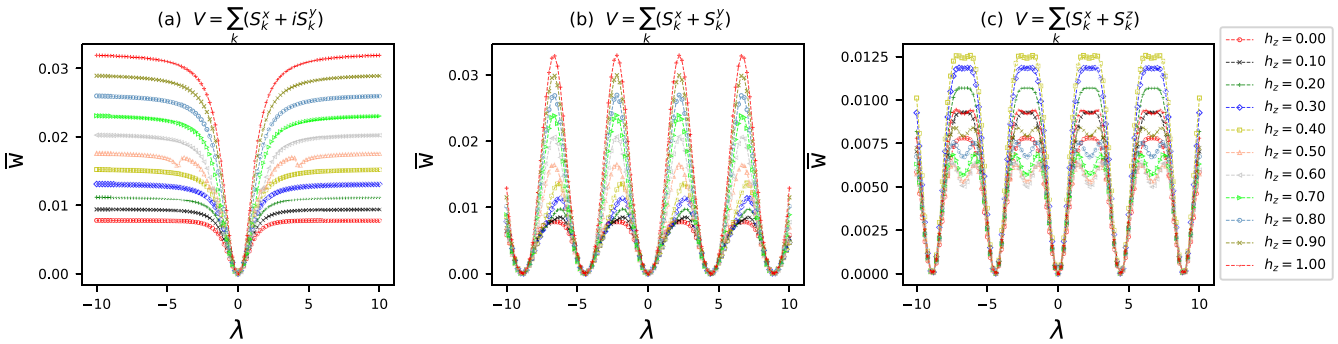

FIG. 15. Plot of $\overline{w}^{\text{impulse}}$ to show the passivity of ground states and its pattern as a function of the coupling λ of an $n=1024$ quantum Ising chain. We fix $h_x=0$ but vary $h_z\in[0,1]$ to obtain various ground states, and we also vary $\lambda\in[-10,10]$ under the impulse process implemented by the Hamiltonian of Eqs. (11) and (13) with the non-Hermitian actions (a) $V=\sum_k(S_k^x+iS_k^y)$, (b) $V=\sum_k(S_k^y+S_k^y)$, and (c) $V=\sum_k(S_k^x+S_k^z)$.

expectation value (VEV) of the Hamiltonian offset using Eq. (16). We check the agreement of the results from both methods for the quantum Ising and Haldane chains of $n=10$ by ED or $n=1024$ by the MPS-based method, as shown in Figs. 13 and 14, respectively.

In Fig. 13 for the quantum Ising model with various h_z in the initial Hamiltonian H_0 under sudden quench process with $V=\sum_k S_k^z$ and $\Delta\lambda=0.01$, we show that the numerical agreement of the numerical results of $\overline{W^m}$ for $m=1,2,3,4$ is obtained from the characteristic function $G(-is)$ (red crosses) or from the VEV of V^m (blue circles). This serves as a consistency check for the TEBD method.

In Fig. 14 for an $n=1024$ Haldane (XXZ) chain with various coupling D in the initial Hamiltonian H_0 under sudden quench process with $V=\sum_k(S_k^z)^2$ and $\Delta\lambda=0.01$, we show the results for (a) $\overline{W}$, (b) $\overline{W^2}$, (c) σ_W^2, and (d) entanglement entropy S, which are obtained from the characteristic function $G(-is)$ (black dashed line for $\chi_{\text{cut}}=32$ or solid line for $\chi_{\text{cut}}=64$) or from the VEV of V^m (red crosses for $\chi_{\text{cut}}=64$ or blue circles $\chi_{\text{cut}}=64$). We can see that the results from both methods match well for (a) and (c) but not for (b). This mismatch can be due to the need of large χ_{cut} to compensate for the errors of performing numerical derivatives on $G(-is)$. This is seen from the improvement of $\overline{W^2}$ in (b) and S in (d) when enlarging χ_{cut} twice large.

APPENDIX C: MORE RESULTS FOR EXAMINING THE PASSIVITY OF GROUND STATES IN ISING-LIKE AND HALDANE-LIKE CHAINS

In this Appendix, we present more results of examining the passivity of the ground states. The first one is shown in Fig. 15 for the plot of $\overline{W}^{\text{impulse}}$ of Ising-like chains as a function of $\lambda\in[-10,10]$ for the more general non-Hermitian actions. It can be seen as the non-Hermitian counterpart of Fig. 10.

Then, we present the Haldane-chain counterparts of Figs. 9 and 10, respectively, in Figs. 16 and 17. Figure 16 shows the plot of $\overline{W}^{\text{impulse}}$ as a function of coupling parameter D labeling the ground states of the Haldane-like chains under various Hermitian actions for small values of $\lambda=0.1$. Figure 17 shows the plot of $\overline{W}^{\text{impulse}}$ as a function of λ to examine the passivity of the ground states under either the Hermitian or non-Hermitian actions of a cyclic impulse process. The key features are similar to what we have observed in Figs. 9 and 10 of the main text for the Ising chains. In particular, the ground states are all passive for all the cases considered. Moreover, the features shown in Fig. 17 are sort of the mixtures of the top and bottom rows in Fig. 10 as the V's considered here are the mixtures of those twos.

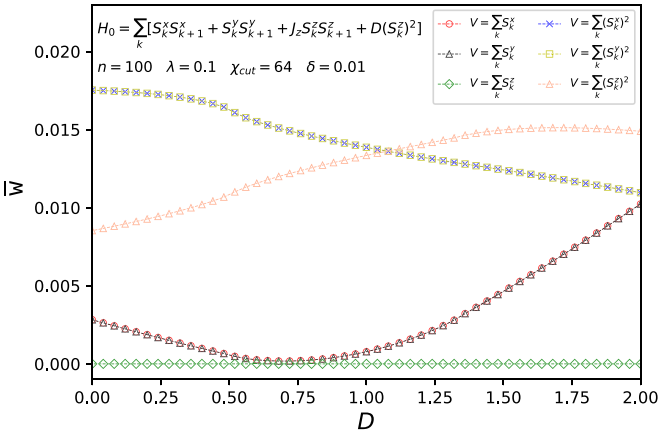

FIG. 16. Plot of $\overline{w}^{\text{impulse}}$ to show the passivity of the ground states of an $n=1024$ Haldane-like chain with $J_z=1.5$ but varying $D\in[0,2]$ under an impulse process of $\lambda=0.1$ and Hermitian actions $V=\sum_k S_k^x$ (black triangles), $\sum_k S_k^y$ (yellow right-arrows), $\sum_k S_k^z$ (red circles), $\sum_k(S_k^x)^2$ (green diamonds), $\sum_k(S_k^y)^2$ (orange left-arrows), and $\sum_k(S_k^z)^2$ (blue squares). The $\overline{W}^{\text{impluse}}$ plots show that the ground states are always passive for all considered V's. The degeneracy of $\overline{W}^{\text{impluse}}$ under swapping of S_i^x and S_i^y, as shown here, can be understood as the Z_2 symmetry of H_0 and SO(3) spin algebra under the transformation $(S_k^x,S_k^y,S_k^z)\to(-S_k^y,S_k^x,S_k^z)$. In addition, $\overline{W}^{\text{impluse}}$ always vanishes for $V=\sum_k S_k^z$ because of $[H_0,\sum_k S_k^z]=0$.

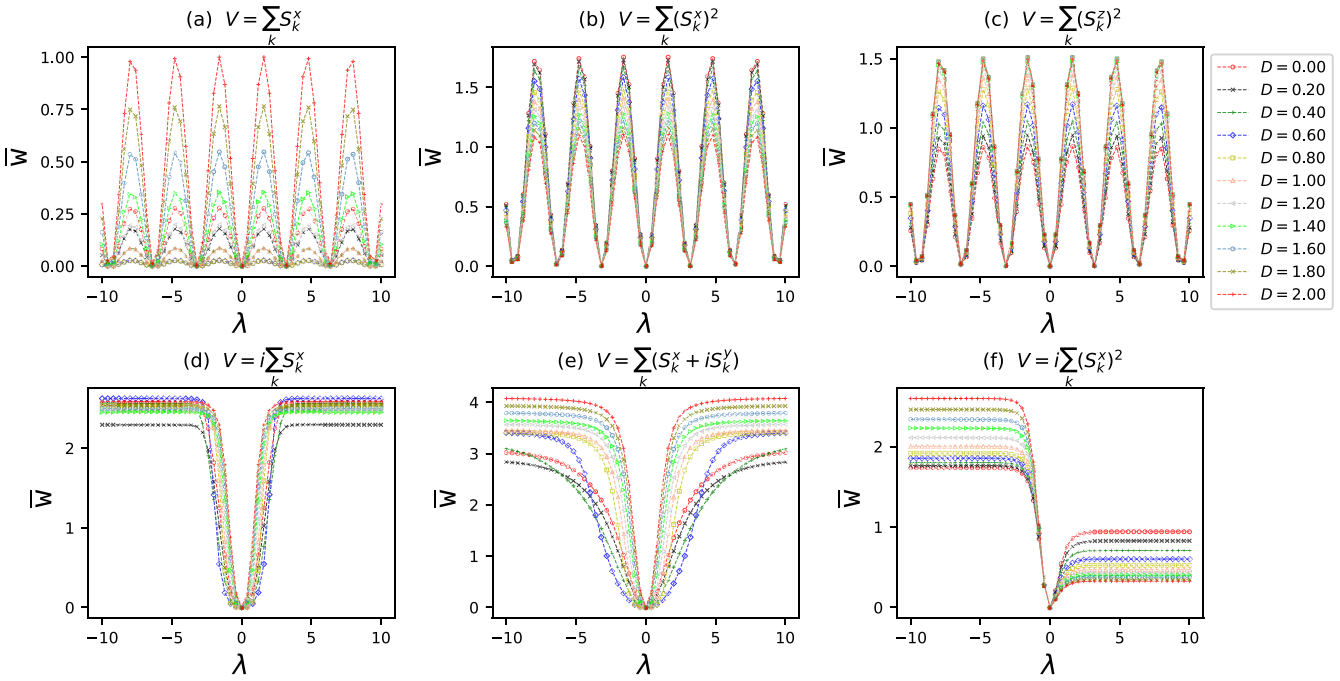

FIG. 17. Plot of $\overline{w}^{\text{impulse}}$ to show the passivity of ground states and its pattern as a function of the coupling λ of $n = 1024$ Haldane-like chain with $J_z = 1.5$. We vary the coupling $D \in [0, 2]$ to obtain various ground states, and we also vary $\lambda \in [-10, 10]$ under the impulse process implemented by the Hamiltonian of Eqs. (11) and (13) for the Hermitian actions (a) $V = \sum_k S_k^x$, (b) $V = \sum_k (S_k^x)^2$, and (c) $V = \sum_k (S_k^z)^2$ in the top row, and the non-Hermitian actions (d) $V = i\sum_k S_k^x$, (e) $V = \sum_k (S_k^x + iS_k^y)$, and (f) $V = i\sum_k (S_k^x)^2$ in the bottom row.

[1] I. Bloch, J. Dalibard, and W. Zwerger, Many-body physics with ultracold gases, Rev. Mod. Phys. **80**, 885 (2008).

[2] I. M. Georgescu, S. Ashhab, and F. Nori, Quantum simulation, Rev. Mod. Phys. **86**, 153 (2014).

[3] C. Gross and I. Bloch, Quantum simulations with ultracold atoms in optical lattices, Science **357**, 995 (2017).

[4] C. Monroe, W. C. Campbell, L.-M. Duan, Z.-X. Gong, A. V. Gorshkov, P. W. Hess, R. Islam, K. Kim, N. M. Linke, G. Pagano *et al.*, Programmable quantum simulations of spin systems with trapped ions, Rev. Mod. Phys. **93**, 025001 (2021).

[5] P. Scholl, M. Schuler, H. J. Williams, A. A. Eberharter, D. Barredo, K.-N. Schymik, V. Lienhard, L.-P. Henry, T. C. Lang, T. Lahaye *et al.*, Quantum simulation of 2d antiferromagnets with hundreds of Rydberg atoms, Nature (London) **595**, 233 (2021).

[6] M. Srednicki, Thermal fluctuations in quantized chaotic systems, J. Phys. A **29**, L75 (1996).

[7] S. Popescu, A. J. Short, and A. Winter, Entanglement and the foundations of statistical mechanics, Nat. Phys. **2**, 754 (2006).

[8] S. Goldstein, J. L. Lebowitz, R. Tumulka, and N. Zanghi, Canonical typicality, Phys. Rev. Lett. **96**, 050403 (2006).

[9] A. Polkovnikov, K. Sengupta, A. Silva, and M. Vengalattore, Nonequilibrium dynamics of closed interacting quantum systems, Rev. Mod. Phys. **83**, 863 (2011).

[10] H. Aoki, N. Tsuji, M. Eckstein, M. Kollar, T. Oka, and P. Werner, Nonequilibrium dynamical mean-field theory and its applications, Rev. Mod. Phys. **86**, 779 (2014).

[11] E. Altman and R. Vosk, Universal dynamics and renormalization in many-body-localized systems, Annu. Rev. Condens. Matter Phys. **6**, 383 (2015).

[12] L. D'Alessio, Y. Kafri, A. Polkovnikov, and M. Rigol, From quantum chaos and eigenstate thermalization to statistical mechanics and thermodynamics, Adv. Phys. **65**, 239 (2016).

[13] F. Alet and N. Laflorencie, Many-body localization: An introduction and selected topics, C. R. Phys. **19**, 498 (2018).

[14] C. Jarzynski, Nonequilibrium equality for free energy differences, Phys. Rev. Lett. **78**, 2690 (1997).

[15] J. Kurchan, Fluctuation theorem for stochastic dynamics, J. Phys. A **31**, 3719 (1998).

[16] G. E. Crooks, Entropy production fluctuation theorem and the nonequilibrium work relation for free energy differences, Phys. Rev. E **60**, 2721 (1999).

[17] H. Tasaki, Jarzynski relations for quantum systems and some applications, arXiv:cond-mat/0009244.

[18] J. Kurchan, A quantum fluctuation theorem, arXiv:cond-mat/0007360.

[19] P. Talkner, E. Lutz, and P. Hänggi, Fluctuation theorems: Work is not an observable, Phys. Rev. E **75**, 050102(R) (2007).

[20] T. Albash, D. A. Lidar, M. Marvian, and P. Zanardi, Fluctuation theorems for quantum processes, Phys. Rev. E **88**, 032146 (2013).

[21] Z. Gong and H. T. Quan, Jarzynski equality, crooks fluctuation theorem, and the fluctuation theorems of heat for arbitrary initial states, Phys. Rev. E **92**, 012131 (2015).

[22] Á. M. Alhambra, L. Masanes, J. Oppenheim, and C. Perry, The second law of quantum thermodynamics as an equality, Phys. Rev. X **6**, 041017 (2016).
[23] J. Åberg, Fully quantum fluctuation theorems, Phys. Rev. X **8**, 011019 (2018).
[24] Z. Fei and H. T. Quan, Nonequilibrium Green's function's approach to the calculation of work statistics, Phys. Rev. Lett. **124**, 240603 (2020).
[25] J. Maldacena, S. H. Shenker, and D. Stanford, A bound on chaos, J. High Energy Phys. 08 (2016) 106.
[26] N. Yunger Halpern, Jarzynski-like equality for the out-of-time-ordered correlator, Phys. Rev. A **95**, 012120 (2017).
[27] N. Yunger Halpern, B. Swingle, and J. Dressel, Quasiprobability behind the out-of-time-ordered correlator, Phys. Rev. A **97**, 042105 (2018).
[28] J. Gu, F. Zhang, and H. T. Quan, Tensor-network approach to work statistics for one-dimensional quantum lattice systems, Phys. Rev. Res. **4**, 033193 (2022).
[29] S. Östlund and S. Rommer, Thermodynamic limit of density matrix renormalization, Phys. Rev. Lett. **75**, 3537 (1995).
[30] G. Vidal, Efficient simulation of one-dimensional quantum many-body systems, Phys. Rev. Lett. **93**, 040502 (2004).
[31] M. Popovic, M. T. Mitchison, A. Strathearn, B. W. Lovett, J. Goold, and P. R. Eastham, Quantum heat statistics with time-evolving matrix product operators, PRX Quantum **2**, 020338 (2021).
[32] V. Murg, F. Verstraete, and J. I. Cirac, Variational study of hard-core bosons in a two-dimensional optical lattice using projected entangled pair states, Phys. Rev. A **75**, 033605 (2007).
[33] A. Silva, Statistics of the work done on a quantum critical system by quenching a control parameter, Phys. Rev. Lett. **101**, 120603 (2008).
[34] A. Chenu, J. Molina-Vilaplana, and A. Del Campo, Work statistics, loschmidt echo and information scrambling in chaotic quantum systems, Quantum **3**, 127 (2019).
[35] E. Mascarenhas, H. Bragança, R. Dorner, M. França Santos, V. Vedral, K. Modi, and J. Goold, Work and quantum phase transitions: Quantum latency, Phys. Rev. E **89**, 062103 (2014).
[36] A. del Campo, Universal statistics of topological defects formed in a quantum phase transition, Phys. Rev. Lett. **121**, 200601 (2018).
[37] Z. Fei, N. Freitas, V. Cavina, H. T. Quan, and M. Esposito, Work statistics across a quantum phase transition, Phys. Rev. Lett. **124**, 170603 (2020).
[38] F. J. Gómez-Ruiz, D. Subires, and A. del Campo, Role of boundary conditions in the full counting statistics of topological defects after crossing a continuous phase transition, Phys. Rev. B **106**, 134302 (2022).
[39] F. Zhang and H. T. Quan, Work statistics across a quantum critical surface, Phys. Rev. E **105**, 024101 (2022).
[40] K. Zawadzki, R. M. Serra, and I. D'Amico, Work-distribution quantumness and irreversibility when crossing a quantum phase transition in finite time, Phys. Rev. Res. **2**, 033167 (2020).
[41] A. D. Varizi, A. P. Vieira, C. Cormick, R. C. Drumond, and G. T. Landi, Quantum coherence and criticality in irreversible work, Phys. Rev. Res. **2**, 033279 (2020).
[42] T. J. Osborne and M. A. Nielsen, Entanglement in a simple quantum phase transition, Phys. Rev. A **66**, 032110 (2002).
[43] C.-Y. Huang and F.-L. Lin, Multipartite entanglement measures and quantum criticality from matrix and tensor product states, Phys. Rev. A **81**, 032304 (2010).
[44] K. Zawadzki, G. A. Canella, V. V. França, and I. D'Amico, Work statistics and entanglement across the fermionic superfluid-insulator transition, Adv. Quantum Technol. **7**, 2300237 (2023).
[45] W. Pusz and S. L. Woronowicz, Passive states and KMS states for general quantum systems, Commun. Math. Phys. **58**, 273 (1978).
[46] A. Lenard, Thermodynamical proof of the Gibbs formula for elementary quantum systems, J. Stat. Phys. **19**, 575 (1978).
[47] S. Goldstein, T. Hara, and H. Tasaki, The second law of thermodynamics for pure quantum states, arXiv:1303.6393.
[48] R. Kubo, Statistical mechanical theory of irreversible processes. I. General theory and simple applications in magnetic and conduction problems, J. Phys. Soc. Jpn. **12**, 570 (1957).
[49] P. C. Martin and J. S. Schwinger, Theory of many particle systems. I, Phys. Rev. **115**, 1342 (1959).
[50] A. E. Allahverdyan, R. Balian, and T. M. Nieuwenhuizen, Maximal work extraction from finite quantum systems, Europhys. Lett. **67**, 565 (2004).
[51] P. Skrzypczyk, A. J. Short, and S. Popescu, Work extraction and thermodynamics for individual quantum systems, Nat. Commun. **5**, 4185 (2014).
[52] M. Frey, K. Funo, and M. Hotta, Strong local passivity in finite quantum systems, Phys. Rev. E **90**, 012127 (2014).
[53] K. Kaneko, E. Iyoda, and T. Sagawa, Work extraction from a single energy eigenstate, Phys. Rev. E **99**, 032128 (2019).
[54] M. Srednicki, Chaos and quantum thermalization, Phys. Rev. E **50**, 888 (1994).
[55] J. M. Deutsch, Quantum statistical mechanics in a closed system, Phys. Rev. A **43**, 2046 (1991).
[56] F.-L. Lin, H. Wang, and J.-j. Zhang, Thermality and excited state Rényi entropy in two-dimensional CFT, J. High Energy Phys. 11 (2016) 116.
[57] S. He, F.-L. Lin, and J.-j. Zhang, Dissimilarities of reduced density matrices and eigenstate thermalization hypothesis, J. High Energy Phys. 12 (2017) 073.
[58] S. He, F.-L. Lin, and J.-j. Zhang, Subsystem eigenstate thermalization hypothesis for entanglement entropy in CFT, J. High Energy Phys. 08 (2017) 126.
[59] F. Roccati, G. M. Palma, F. Ciccarello, and F. Bagarello, Non-Hermitian physics and master equations, Open Syst. Inf. Dyn. **29**, 2250004 (2022).
[60] A. W. Schlimgen, K. Head-Marsden, L. M. Sager-Smith, P. Narang, and D. A. Mazziotti, Quantum state preparation and nonunitary evolution with diagonal operators, Phys. Rev. A **106**, 022414 (2022).
[61] O. A. Castro-Alvaredo and A. Fring, A spin chain model with non-Hermitian interaction: the Ising quantum spin chain in an imaginary field, J. Phys. A **42**, 465211 (2009).
[62] G. Vidal, Classical simulation of infinite-size quantum lattice systems in one spatial dimension, Phys. Rev. Lett. **98**, 070201 (2007).
[63] R. Orús and G. Vidal, Infinite time-evolving block decimation algorithm beyond unitary evolution, Phys. Rev. B **78**, 155117 (2008).

[64] E. Stoudenmire and S. R. White, Minimally entangled typical thermal state algorithms, New J. Phys. **12**, 055026 (2010).

[65] M. Henkel, *Conformal Invariance and Critical Phenomena*, Theoretical and Mathematical Physics (Springer, Berlin, 2013).

[66] F. A. Bayocboc, Jr. and F. N. C. Paraan, Exact work statistics of quantum quenches in the anisotropic XY model, Phys. Rev. E **92**, 032142 (2015).

[67] Y. Hatsugai and M. Kohmoto, Numerical study of the Hidden antiferromagnetic order in the Haldane phase, Phys. Rev. B **44**, 11789 (1991).

[68] W. Chen, K. Hida, and B. C. Sanctuary, Ground-state phase diagram of $S = 1$ XXZ chains with uniaxial single-ion-type anisotropy, Phys. Rev. B **67**, 104401 (2003).